Two-Year Dynamical Predictions of ENSO Event Duration during 1954–2015

XIAN WU,[a] YUKO M. OKUMURA,[a] CLARA DESER,[b] AND PEDRO N. DINEZIO[c]

[a] *Institute for Geophysics, Jackson School of Geosciences, The University of Texas at Austin, Austin, Texas*
[b] *Climate and Global Dynamics Division, National Center for Atmospheric Research, Boulder, Colorado*
[c] *Department of Atmospheric and Oceanic Sciences, University of Colorado Boulder, Boulder, Colorado*

(Manuscript received 5 August 2020, in final form 7 February 2021)

ABSTRACT: El Niño and La Niña events show a wide range of durations over the historical record. The predictability of event duration has remained largely unknown, although multiyear events could prolong their climate impacts. To explore the predictability of El Niño and La Niña event duration, multiyear ensemble forecasts are conducted with the Community Earth System Model, version 1 (CESM1). The 10–40-member forecasts are initialized with observed oceanic conditions on 1 March, 1 June, and 1 November of each year during 1954–2015; ensemble spread is created through slight perturbations to the atmospheric initial conditions. The CESM1 predicts the duration of individual El Niño and La Niña events with lead times ranging from 6 to 25 months. In particular, forecasts initialized in November, near the first peak of El Niño or La Niña, can skillfully predict whether the event continues through the second year with 1-yr lead time. The occurrence of multiyear La Niña events can be predicted even earlier with lead times up to 25 months, especially when they are preceded by strong El Niño. The predictability of event duration arises from initial thermocline depth anomalies in the equatorial Pacific, as well as sea surface temperature anomalies within and outside the tropical Pacific. The forecast error growth, on the other hand, originates mainly from atmospheric variability over the North Pacific in boreal winter. The high predictability of event duration indicates the potential for extending 12-month operational forecasts of El Niño and La Niña events by one additional year.

KEYWORDS: Pacific Ocean; Tropics; Atmosphere-ocean interaction; ENSO; Climate prediction

1. Introduction

The El Niño–Southern Oscillation (ENSO) phenomenon arises from dynamic and thermodynamic interactions of the ocean and atmosphere in the tropical Pacific and is the largest source of climate variability on interannual time scales (e.g., Wallace et al. 1998; Neelin et al. 1998; Wang and Picaut 2004; Chang et al. 2006). Anomalously warm (El Niño) and cold (La Niña) sea surface temperature (SST) conditions in the central and eastern equatorial Pacific associated with ENSO alter the distribution of atmospheric convection in the tropics and influence global weather patterns via atmospheric teleconnections (e.g., Trenberth et al. 1998; Alexander et al. 2002; Taschetto et al. 2020). Climate forecast centers around the world have been making routine ENSO predictions since the 1980s, which provide the basis for seasonal forecasts of temperature and precipitation over North America and Europe (e.g., Kumar and Hoerling 2000; Shukla et al. 2000; Kumar et al. 2014; Scaife et al. 2014; L'Heureux et al. 2015, 2020). Early studies on ENSO prediction focused on the onset and amplitude of ENSO events (Latif et al. 1998; Kirtman et al. 2002; Chen and Cane 2008; Jin et al. 2008). More recent research has expanded to include predictions of the spatial pattern of ENSO-related SST anomalies throughout the tropical Pacific basin (Hendon et al. 2009; Capotondi et al. 2015; Imada et al. 2015). Long-range forecasts of the duration of ENSO events have, however, received much less attention, with only a few case studies focused on multiyear La Niña events and a single initialization month (DiNezio et al. 2017a,b; Luo et al. 2017). The duration of ENSO events could affect the length of their associated climate and socioeconomic impacts (e.g., Hoerling and Kumar 2003; Okumura et al. 2017; Deepak et al. 2019), calling for accurate predictions of ENSO event duration with sufficient lead times.

Recent progress has been made in understanding the characteristics and mechanisms of ENSO event duration. ENSO events usually start to develop during boreal spring to summer and peak in boreal winter. After the peak, individual ENSO events show a wide range of temporal evolution in the subsequent year. About one in three El Niño events and one out of two La Niña events persist for a second year (Wu et al. 2019). Multiyear events account for a larger fraction for La Niña than El Niño events, in agreement with the longer average duration of La Niña than El Niño shown by previous studies (Kessler 2002; Larkin and Harrison 2002; McPhaden and Zhang 2009; Ohba and Ueda 2009; Okumura and Deser 2010; Wu et al. 2010; Dommenget et al. 2013; An et al. 2020). Previous studies suggest that the primary factor controlling the duration of individual El Niño events is the onset timing (Horii and Hanawa 2004; Lee et al. 2014; Wu et al. 2019), while the duration of individual La Niña events is strongly affected by the amplitude of preceding warm event (DiNezio and Deser 2014; Wu et al. 2019). These factors influence the duration of individual ENSO events by modulating the timing and magnitude of negative feedbacks within the tropical Pacific, as well as from the other

Denotes content that is immediately available upon publication as open access.

Supplemental information related to this paper is available at the Journals Online website: https://doi.org/10.1175/JCLI-D-20-0619.s1.

Corresponding author: Dr. Xian Wu, xianwu@ucar.edu

DOI: 10.1175/JCLI-D-20-0619.1

tropical oceans. El Niño events that develop early in boreal summer tend to terminate shortly after their peak in boreal winter, whereas those that develop in late boreal summer to fall usually last two years. The early onset timing of El Niño leads to the earlier occurrence of Rossby wave reflection and sooner adjustment of tropical Atlantic and Indian Oceans by the mature phase, both of which effectively terminate the event by the following summer (Wu et al. 2019). In the meantime, when La Niña follows strong El Niño, initial large thermocline shoaling across the equatorial Pacific and strong warming of the Atlantic and Indian Oceans together act to prolong the La Niña duration, with the latter enhancing easterly wind anomalies over the western Pacific (DiNezio and Deser 2014; Wu et al. 2019).

Do the long-lead precursors and associated dynamical mechanisms for ENSO event duration indicate its degree of predictability? The potential predictability of ENSO event duration has been explored in the perfect model predictions conducted with the Community Earth System Model, version 1 (CESM1; Kay et al. 2015), a climate model that realistically simulates the diverse temporal evolution of ENSO events (DiNezio et al. 2017a; Wu et al. 2021). In these idealized prediction experiments, the model predicts its own trajectories in the control simulation with perfect initialization of oceanic, sea ice, and land states and with roundoff level errors added to atmospheric initial conditions. Thus, these predictions are not affected by the issues common in the operational ENSO forecasts, including the errors in initial conditions and model drift to its own climatology. Under the perfect model setting, the CESM1 successfully predicts the termination of early-onset El Niño and the multiyear persistence of late-onset El Niño when initialized with oceanic conditions in the onset months (Wu et al. 2021). Multiyear La Niña can also be predicted when the CESM1 is initialized around the peak of strong El Niño (DiNezio et al. 2017a).

The real-world prediction skill of ENSO event duration remains largely unexplored other than the case study of the 2017–18 La Niña by DiNezio et al. (2017b). Current operational ENSO forecasts are run forward for up to 12 months (Barnston et al. 2012, 2019), thus precluding forecasts of multiyear ENSO events. In addition, operational forecasts show difficulty predicting the reintensification of multiyear La Niña in winters of 2008, 2011, and 2017, even when initialized in boreal summer before the second La Niña peak (https://iri.columbia.edu/our-expertise/climate/forecasts/enso/archive/). The limited skill of the operational forecasts in predicting the return of La Niña could partly arise from the difficulties of climate models in simulating the asymmetric duration of El Niño and La Niña (Ohba et al. 2010). Using the retrospective forecasts conducted with the CESM1, DiNezio et al. (2017b) showed that multiyear La Niña events during 1954–2015 can be predicted 2 years in advance when the model is initialized with observed oceanic conditions near the peak of strong El Niño events. The predictability of these multiyear La Niña events is attributed to subsurface oceanic memory associated with strong El Niño. However, some multiyear La Niña events follow weak-to-moderate El Niño events (e.g., 1970–72 and 2007–09); conversely, the La Niña event that followed the relatively strong El Niño in 1986–87 lasted only one year. The predictability and underlying mechanisms of these particular La Niña events remain unclear. Moreover, the predictability of El Niño duration in the real world has not yet been investigated.

In this study, we analyze a suite of multiyear ensemble forecasts performed with the CESM1 and initialized with observed oceanic conditions on 1 March, 1 June, and 1 November of each year from 1954 to 2015. The 3×62 ensemble forecasts can provide a more comprehensive assessment of the predictability and mechanisms of observed ENSO event duration at different lead times up to 25 months, as well as an assessment of seasonal dependence of forecast skill. In particular, we address the following questions. To what extent can we predict the duration of El Niño and La Niña events in the real world? What is the maximum lead time of skillful predictions, and what are the mechanisms affecting the predictability and forecast error growth? Is it feasible to extend the current 12-month operational ENSO forecasts by one additional year? The rest of the paper is organized as follows. Section 2 describes the model, forecast experiments, and analysis methods. Section 3 estimates the predictability and error growth of ENSO event duration in the forecasts and investigates the underlying oceanic and atmospheric mechanisms. Section 4 summarizes the main results and discusses the implications for operational ENSO forecasts and outlook for future studies.

2. Model experiments and analysis methods

a. CESM1

We conduct a suite of multiyear ensemble forecasts with the Community Earth System Model, version 1 (CESM1), a state-of-the-art climate model developed at the National Center for Atmospheric Research. The CESM1 consists of atmosphere, ocean, land surface, and sea ice components linked by a flux coupler (Hurrell et al. 2013; Kay et al. 2015). The atmospheric component is the Community Atmosphere Model, version 5 (CAM5) that uses a finite-volume dynamical core at a horizontal resolution of 0.9° latitude $\times$ 1.25° longitude with 30 levels in vertical (Neale et al. 2012). The oceanic component, the Parallel Ocean Program, version 2 (POP2; Smith et al. 2010), has meridional resolutions increasing from 0.65° at 60°N to 0.27° at the equator and 60 levels in the vertical. The land model is version 4 of the Community Land Model (CLM4; Lawrence et al. 2011) that is run on the same horizontal grid as the atmosphere model. The sea ice model, the Los Alamos National Laboratory Community Ice Code, version 4 (Hunke and Lipscomb 2008), uses the same horizontal grid as the ocean model.

The CESM1 reproduces many important characteristics of observed ENSO behavior, including the broad spectral peak in the 3–6-yr band, asymmetries between El Niño and La Niña, and diversity in the amplitude, pattern, and temporal evolution of individual events; however, the CESM1 overestimates the overall amplitude of ENSO by about 20% (DiNezio et al. 2017a; Wu et al. 2019; Capotondi et al. 2020; Planton et al. 2021). Importantly, the CESM1 captures the observed ratio of single and multiyear ENSO events and the associated oceanic

TABLE 1. A summary of the forecast ensembles used in this study. Forecasts are initialized on 1 Mar, 1 Jun, and 1 Nov of each year during 1954–2015.

Initialization month	Simulation length	Ensemble size	Ocean and sea ice initial conditions	Atmosphere and land initial conditions
March	30 months	10	CORE-forced FOSI	FOSI-forced CAM5-CLM4
June	27 months	20	CORE-forced FOSI	FOSI-forced CAM5-CLM4
November	122 months	40	CORE-forced FOSI	CESM1 uninitialized

and atmospheric mechanisms (Wu et al. 2019). Nevertheless, ENSO anomalies simulated in the CESM1 show an excessive extension to the western equatorial Pacific than observed (Capotondi et al. 2020), which is a common problem among climate models and related to too cold climatological SST in the equatorial Pacific (e.g., Bellenger et al. 2014; Graham et al. 2017; Planton et al. 2021). The potential effect of these model biases on our forecasts of ENSO event duration will be briefly discussed in section 3b.

b. Forecast experiments

To explore the predictability of ENSO event duration at different lead times, we analyze CESM1 multiyear ensemble forecasts initialized with observed oceanic conditions on 1 March, 1 June, and 1 November in each year during 1954–2015 (Table 1). The forecasts initialized in November are part of the CESM Decadal Prediction Large Ensemble (CESM-DPLE; Yeager et al. 2018), which consists of 40 members of 10-yr simulations for each initialization year. We use the first 30 months of forecasts from the CESM-DPLE for our analysis. Following the CESM-DPLE protocol, we conduct two additional sets of ensemble forecasts initialized on 1 March and 1 June of each year. The March- and June-initialized forecasts are integrated for 30 and 27 months, respectively, and consist of 10 and 20 members for each initialization year, respectively. The three initialization months correspond to the peak, decay, and onset phases of ENSO events, and the comparison of forecasts initialized before and after spring can show the influence of the spring predictability barrier. The bootstrap analysis of 40-member November-initialized forecasts suggests that an ensemble size of 10 is sufficient to estimate the ensemble mean and spread for 2-yr lead forecasts (see Fig. S2 in the online supplemental material).

In all three sets of forecasts, each ensemble is initialized with the same ocean and sea ice conditions obtained from a simulation in which the ocean and sea ice components of CESM1 are forced with observed atmospheric and surface flux fields [hereafter called a forced ocean–sea ice simulation (FOSI)]. The surface fluxes are computed using bulk formulas based on observed atmospheric fields from the Coordinated Ocean-Ice Reference Experiment (CORE) forcing dataset (Yeager et al. 2015). Please refer to Yeager et al. (2018) for details of the ocean and sea ice initialization. The atmosphere and land initial conditions for the CESM-DPLE are based on one ensemble member of the CESM Large Ensemble Project (Kay et al. 2015), in which ocean and sea ice conditions evolve freely. For the March- and June-initialized forecasts, the atmosphere and land initial conditions are generated using a CAM5-CLM4 simulation forced with observed monthly ocean and sea ice fields from the FOSI. This change in the initialization scheme was introduced to produce more realistic land initial conditions over the tropics and midlatitude areas where atmospheric conditions are strongly controlled by SST forcing. A more accurate initialization of land features (e.g., soil moisture) may improve predictions of hydroclimate variability over land. However, we expect that most of the predictability of ENSO events arises from oceanic initial states due to its long memory. All ensemble members were initialized with atmospheric initial conditions modified with a unique perturbation at the roundoff level of the computer (order 10^{-14}). The smallest possible perturbations result in entirely uncorrelated weather after about a week among the members, generating the ensemble spread. All forecasts are run under the Coupled Model Intercomparison Project phase 5 (CMIP5) "historical" forcing for 1954–2005 and the CMIP5 representative concentration pathway 8.5 forcing for 2006–15. Table 1 summarizes the information on the forecast ensembles used in this study.

c. Drift correction and detrending methods

Because the CESM1 does not perfectly reproduce the observed climatology, the observed initial conditions cause the model to drift toward its own climatology as the simulation proceeds. To remove this effect, a given output variable from the ensemble forecast, Y, is adjusted following a method that has been extensively used for correcting the full-field initialization forecasts (CLIVAR 2011; Meehl and Teng 2012; Yeager et al. 2012; Hazeleger et al. 2013). For each ensemble mean forecasts initialized in year j, the variable Y is averaged across members 1 to m for lead time τ (1.1). The resulting ensemble mean variable is then averaged across all initialization years to obtain a "drifting" baseline as a function of lead time (1.2). The "drifting climatology" is then subtracted from each member in each ensemble to yield drift-adjusted anomalies (1.3):

$$Y_{j\tau} = \frac{1}{m}\sum_{k=1}^{m} Y_{jk\tau}, \tag{1.1}$$

$$\overline{Y_{\tau}} = \frac{1}{n}\sum_{j=1}^{n} Y_{j\tau}, \tag{1.2}$$

$$Y'_{jk\tau} = Y_{jk\tau} - \overline{Y_{\tau}}, \tag{1.3}$$

Here, $Y_{jk\tau}$ represents a given variable Y at lead time τ from a member k of an ensemble initialized in year j, $Y_{j\tau}$ is the ensemble mean of $Y_{jk\tau}$, and $\overline{Y_{\tau}}$ is the "drifting" baseline common to all ensemble members; $Y'_{jk\tau}$ is the drift-corrected $Y_{jk\tau}$. The "drifting climatology" is calculated for the period of 1958–2015 for each lead time, to be consistent with the period of observational data used for forecast verification. To remove the

TABLE 2. A list of 1- and 2-yr El Niño and La Niña events during 1954–2015, denoted by the years when the events first develop.

	Years
1-yr El Niño	1963, 1965, 1972, 1982, 1991, 1994, 1997, 2002, 2006, 2009
2-yr El Niño	1957, 1968, 1976, 1986, 2014
1-yr La Niña	1964, 1988, 1995, 2005
2-yr La Niña	1954, 1970, 1973, 1983, 1998, 2007, 2010, 2016

effect of global warming, we calculate the quadratic trend of ensemble means at each lead time and subtract it from each ensemble member.

d. Observational data and forecast verification

The forecasts of ENSO events are verified against several observational datasets through composite and correlation analyses. For SST, we use the Hadley Centre Sea Ice and SST dataset (Rayner et al. 2003) available for 1870–2019 on a 1° grid. The thermocline depth, which is defined as the depth of maximum vertical temperature gradient, is derived from the European Centre for Medium-Range Weather Forecasts (ECMWF) Ocean Reanalysis System 4 (Balmaseda et al. 2013) available for 1958–2017 on a 1° grid with 42 levels in the vertical. For surface wind components, we make use of the National Centers for Environmental Prediction (NCEP)–National Center for Atmospheric Research (NCAR) reanalysis (Kalnay et al. 1996) available for 1948–2017 on a 2.5° grid. As for the ensemble forecasts, observed monthly climatology is calculated for 1958–2015 and monthly anomalies are quadratically detrended.

We select observed ENSO events for forecast verification based on SST anomalies averaged over the Niño-3.4 region (170°–120°W, 5°S–5°N; hereafter called the Niño-3.4 index). The year when an ENSO event first develops is denoted as year 0 and the months of the year, using the first three letters of each month name, as Jan^0, Feb^0, . . . , and so on to Dec^0. Following Wu et al. (2019), El Niño and La Niña events are defined when the Niño-3.4 index smoothed with a 3-month running mean filter is greater than 0.75 standard deviations and less than −0.75 standard deviations in any month from Oct^0 to Feb^{+1} (i.e. February of the following year), respectively. The standard deviation of the smoothed Niño-3.4 index is calculated separately for each month, ranging from 0.89° to 1.09°C during October–February. El Niño and La Niña events are further classified into 2-yr events when the smoothed Niño-3.4 index remains above 0.5 standard deviations and less than −0.5 standard deviations in any month from Oct^{+1} to Feb^{+2}, respectively, and otherwise into 1-yr events. The weaker threshold value used for the second compared to the first year is based on the observed features of 1-yr and 2-yr ENSO events (Wu et al. 2019). During the period for which the CESM1 ensemble forecasts are available (1954–2017), there are ten 1-yr El Niño, five 2-yr El Niño, four 1-yr La Niña, and eight 2-yr La Niña events (Table 2). Figure 1 and Fig. S1 show the time series of the Niño-3.4 index in observations and forecasts for individual 1- and 2-yr El Niño/La Niña events.

Using the three sets of CESM1 forecast ensembles initialized in March, June, and November, we examine how far in advance the duration of observed ENSO events can be predicted. The Niño-3.4 index in Dec^{+1} is used as an indicator of the ENSO event duration, and the forecast lead time is defined relative to Dec^{+1}. For simplicity, we use threshold values of 0.5°C and −0.5°C, which is close to 0.5 standard deviation of the Dec^{+1} Niño-3.4 index in CESM1 (0.58°C), to determine the predicted duration of El Niño and La Niña events, respectively. For all El Niño and La Niña events during 1954–2015, we compare the temporal evolution of the Niño-3.4 index between observations and ensemble forecasts initialized in Nov^{-1}, Mar^0, Jun^0, Nov^0, Mar^{+1}, and Jun^{+1}, which give lead times ranging from 25 to 6 months. To assess the ability of CESM1 in predicting the duration of El Niño and La Niña, we compare observed and predicted evolutions of the Niño-3.4 index and other oceanic and atmospheric variables composited for all 1- and 2-yr El Niño and La Niña events. The CESM1's prediction skill is also assessed using the correlation coefficient and root-mean-square error (RMSE) of the Niño-3.4 index between observations and ensemble mean forecasts as a function of lead time. We compare the prediction skill of CESM1 forecasts with the persistence forecasts, which assume that the observed anomaly in the month before initialization remains unchanged for the period of forecasts. We also compare the RMSE with the root-mean-square (RMS) of the observed Niño-3.4 index to assess the prediction skill in terms of relative amplitude. The statistical significance of the composite and correlation analyses is tested through a two-tailed Student's t test at the confidence level of 95% for both observations and forecasts. The relatively small sample size of 2-yr El Niño and 1-yr La Niña events in observations makes it difficult to obtain robust signals. However, the composite features of 1- and 2-yr events are in overall agreement with our previous findings based on the extended period 1900–2017 (Wu et al. 2019).

3. Results

a. Predictability of 1-yr and 2-yr ENSO events

The CESM1 successfully predicts the temporal evolution of ENSO events with lead times up to 25 months, well beyond the maximum lead time of 12 months in the current operational ENSO forecasts. The ensemble forecasts initialized at six different lead times relative to Dec^{+1} are shown for four representative 1- and 2-yr ENSO events in Fig. 1 (see Fig. S1 for all other events). The development and termination of the strong 1-yr El Niño in 1972 are predicted in nearly all members of the ensemble forecasts initialized in Mar^0 with a 21-month lead time, although the subsequent development of La Niña in 1973 is not captured by the ensemble forecasts until the model is initialized in Nov^0. The development of the 2-yr El Niño in 1986–87 is first predicted by the ensemble forecasts initialized in Nov^0 due to the late onset. The Nov^0-initialized forecasts further predict the continuation of El Niño into 1987 in the ensemble mean with a 13-month lead time, consistent with observations. The development and termination of the strong 1-yr La Niña in 1988 are predicted in the ensemble forecasts initialized in Jun^0 with an 18-month lead time. Most prominently, the development and continuation of the multiyear La Niña in 1998–2000 are predicted with a 25-month lead time in the ensemble forecasts initialized as early as in Nov^{-1}, around the peak of the preceding strong El Niño in 1997.

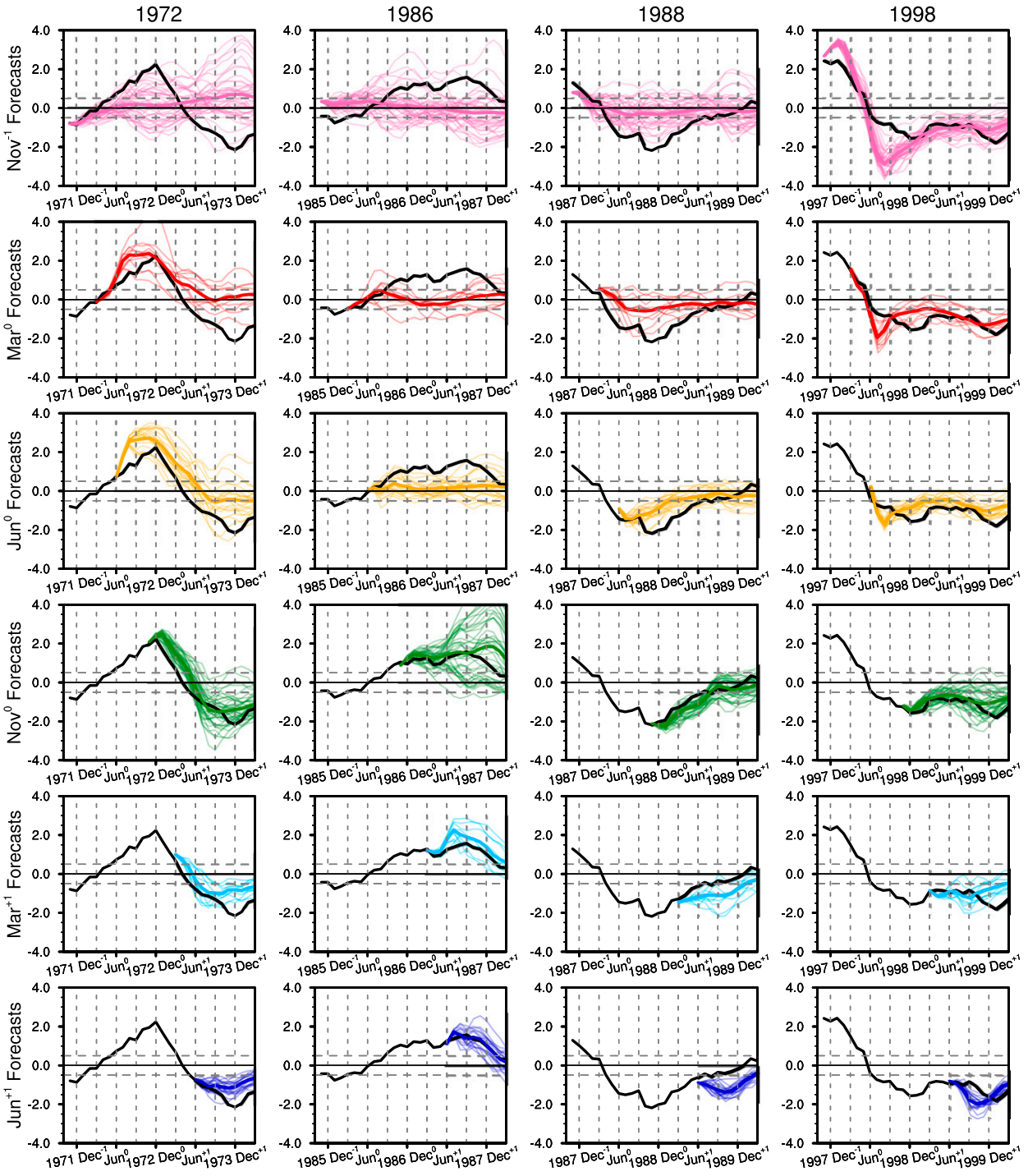

FIG. 1. Time series of the Niño-3.4 index in observations (black curves) and ensemble forecasts (colored curves) for (first column) 1-yr El Niño in 1972, (second column) 2-yr El Niño in 1986–87, (third column) 1-yr La Niña in 1988, and (fourth column) 2-yr La Niña in 1998–99. The ensemble forecasts are initialized in (first row) Nov^{-1}, (second row) Mar^{0}, (third row) Jun^{0}, (fourth row) Nov^{0}, (fifth row) Mar^{+1}, and (sixth row) Jun^{+1}. Dec^{0} denotes the first peak of El Niño/La Niña events. The ensemble mean and individual member forecasts are indicated by the thick and light colored curves, respectively. See Fig. S1 for predictions of all other 1- and 2-yr ENSO events during 1954–2015.

To assess the overall ability of CESM1 in predicting the ENSO event duration, the observed and predicted Niño-3.4 index are composited for all 1-yr and 2-yr El Niño and La Niña events during 1954–2015 (Table 2; Fig. 2, left). On average, the development and termination of both 1-yr El Niño and La Niña composites are predicted in the ensemble forecasts initialized in Jun^0, when these composite events tend to begin. The transition from 1-yr El Niño to La Niña is not predicted until Jun^{+1}, partly due to the CESM1's bias in simulating prolonged El Niño as discussed further in section 3b. The development and continuation of 2-yr El Niño are, on the other hand, predicted by Nov^0, providing up to 13 months of lead time relative to the second peak in Dec^{+1}. The development and continuation of 2-yr La Niña are predicted even one year earlier in Nov^{-1} with lead time of 25 months. The predicted first peak of La Niña occurs too early compared to observations, but this apparent forecast error is an artifact of the extensive westward shift of maximum equatorial cooling during boreal summer-fall in the CESM1 (cf. Fig. 6). The predicted Dec^{+1} Niño-3.4 index for all ensemble forecast members shows a similar frequency distribution for all lead times, indicating high multiyear predictability of 2-yr La Niña (Fig. 2, right). In contrast, the frequency distribution of the Dec^{+1} Niño-3.4 index becomes wider with longer lead times for other event categories. Overall, the CESM1 can predict the event duration for all categories when initialized in Nov^0 with a lead time of 13 months.

We examine the robustness of the composite forecasts by comparing the observed and predicted ensemble-mean Niño-3.4 index in Dec^0 and Dec^{+1} for the individual ENSO events that make up each composite (Fig. 3). The event termination in Dec^{+1} is predicted in the Nov^0-initialized forecasts in seven out of ten 1-yr El Niño events and three out of four 1-yr La Niña events. The forecasts initialized before Nov^0 show a positive bias of the Dec^{+1} Niño-3.4 index for most 1-yr El Niño events, consistent with the composite forecasts (Fig. 2). The event continuation in Dec^{+1} is predicted in the Nov^0-initialized forecasts in four out of five 2-yr El Niño events and in the Nov^{-1}- or Mar^0-initialized forecasts in all 2-yr La Niña events. The notable consistency of multiyear predictability of 2-yr La Niña agrees with the earlier study by DiNezio et al. (2017a,b). It is noted that some forecasts initialized before Nov^0 fail to predict the development of ENSO by Dec^0 and thus are unsuitable for the prediction of ENSO event duration.

Figure 4 shows the correlation skill and RMSE of the Niño-3.4 index predicted by the CESM1 for all years, El Niño years, and La Niña years during 1954–2015. In general, the correlation skill decreases quickly in boreal spring (Mar^0–Jun^0 and Mar^{+1}–Jun^{+1}), reflecting the well-known spring predictability barrier of ENSO (e.g., Torrence and Webster 1998). The CESM1 forecasts show higher correlation skill than the persistence forecasts at most lead times. The correlation skill based on all years remains above 0.5 within 13, 13, and 11 months in the forecasts initialized in Nov^{-1}, Mar^0, and Jun^0, respectively. When the analysis is limited to El Niño years, the Nov^0-initialized forecasts show correlation skills above 0.5 during Dec^{+1}–May^{+2} with 13–18-month lead times, indicating long-range predictability of El Niño duration. The analysis limited to La Niña years shows even higher correlation skill, exceeding 0.8 during Aug^{+1}–Mar^{+2} in the Nov^0-initialized forecasts (9–16-month lead times) and during Dec^{+1}–Feb^{+2} in the Jun^0-initialized forecasts (13–17-month lead times). The correlation skill increases slightly during boreal summer to winter of the second year (Jun^{+1}–Dec^{+1}) of El Niño and La Niña in the forecasts initialized in Nov^0–Jun^{+1}, which may be caused by seasonal growth of predictable SST anomalies [a similar result was reported in Chen et al. (2004)]. The higher prediction skill for La Niña than El Niño years is likely related to the CESM1's error of overestimating the duration of 1-yr El Niño (Fig. 2).

The RMSE of the forecasts, on the other hand, grows rapidly in boreal summer and fall (Jun^0–Nov^0 and Jun^{+1}–Nov^{+1}) due to the seasonal intensification of the Bjerknes feedback (e.g., Neelin et al. 1998). In general, the forecasts show smaller RMSE when the correlation skill is higher. The RMSE is smaller than the RMS of observed Niño-3.4 index in Dec^{+1} when the correlation skill is above 0.6 in the forecasts initialized in and after Nov^0 for El Niño and La Niña years, indicating skillful predictions. These results show that the CESM1 has high predictive skill of ENSO event duration with lead times of more than one year when initialized at certain ENSO states, owing to the model's ability to simulate the dynamical processes associated with ENSO events.

b. *Processes controlling the predictability in the Nov^0-initialized forecasts*

We first analyze the processes contributing to the high predictability of ENSO event duration in the Nov^0-initialized forecasts. Figure 5 compares the composite evolutions of SST, thermocline depth, and surface wind anomalies in the equatorial Pacific between 1- and 2-yr El Niño and La Niña events in observations and the Nov^0-initialized forecasts (see Fig. S3 for the statistical significance of these composites). In observations, SST warming associated with 1-yr El Niño exceeds 0.4°C around May^0 in the western-central Pacific (170°E–160°W), 2–4 months earlier compared to 2-yr El Niño. 1-yr El Niño becomes stronger during the mature phase compared to 2-yr El Niño, with maximum amplitudes ~1.6°C compared to 1.1°C in Dec^0. Because of the earlier onset and stronger peak amplitude, upwelling equatorial Rossby waves that provide negative feedback to the equatorial Pacific warming have larger amplitude and arrive at the western boundary earlier in 1-yr El Niño compared to 2-yr El Niño (Wu et al. 2019). The equatorial thermocline starts to shoal in the western Pacific by late summer of year 0 in 1-yr El Niño, but not until year +1 in 2-yr El Niño; the magnitude of the shoaling is also less for 2-yr El Niño compared to 1-yr El Niño. As a result, thermocline depth anomalies in the western equatorial Pacific are of opposite sign in Nov^0 between 1- and 2-yr El Niño, and the ensemble forecasts initialized in that month show a distinct evolution. In the 1-yr El Niño forecasts, the negative thermocline depth anomalies propagate into the eastern Pacific during boreal spring, leading to a rapid decay of SST anomalies. In the 2-yr El Niño forecasts, by contrast, the delayed propagation of weaker negative thermocline depth anomalies is not sufficient to terminate the event in spring, and the remnant SST warming starts to reintensify during the equatorial cold season (June–November). Thus, the timing and magnitude of delayed

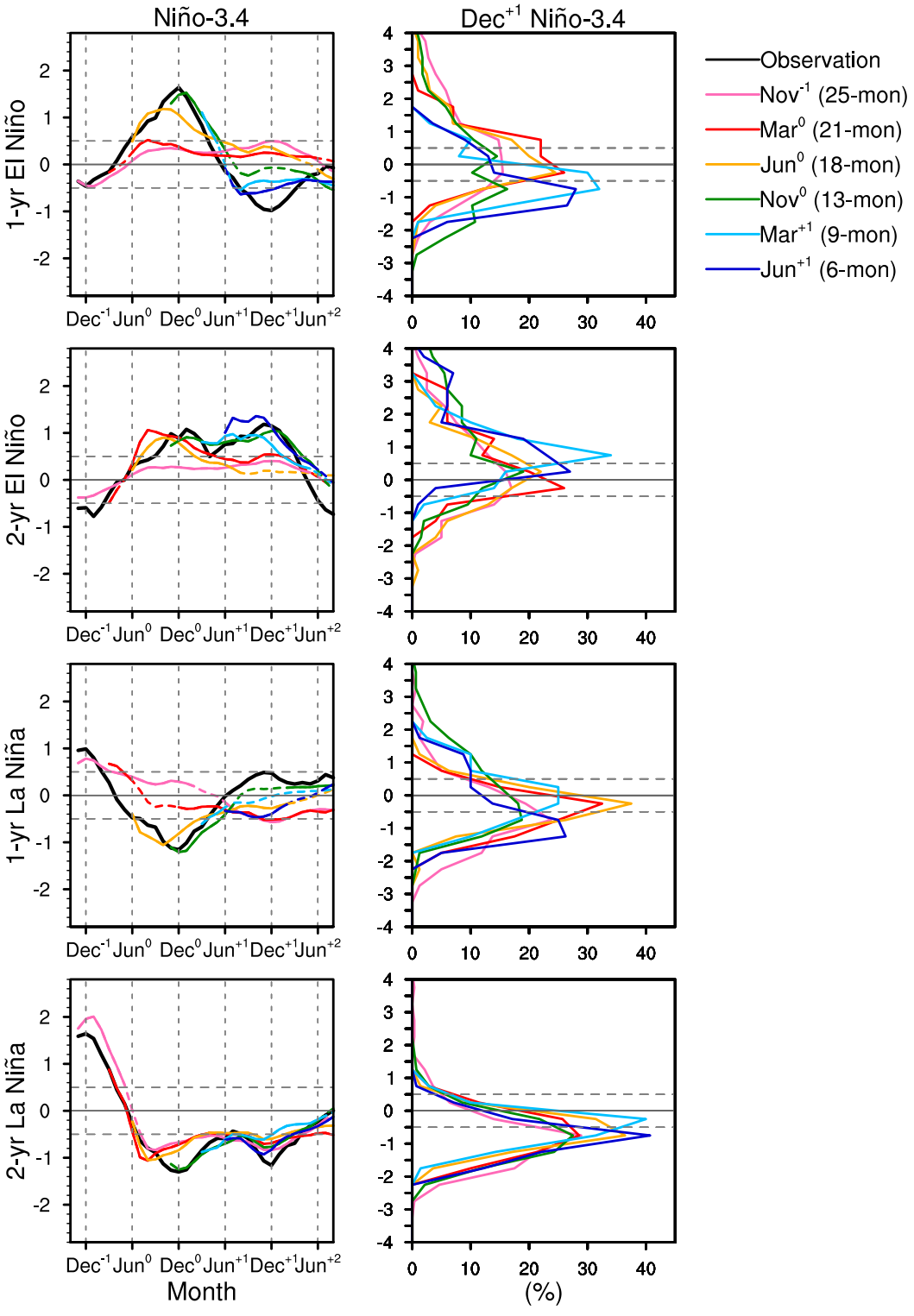

FIG. 2. (left) Time series of the Niño-3.4 index (°C) in observations (black curves) and ensemble-mean forecasts (colored curves) composited for all (first row) 1-yr El Niño, (second row) 2-yr El Niño, (third row) 1-yr La Niña, and (fourth row) 2-yr La Niña events during 1954–2015. The forecasts are initialized in Nov^{-1} (pink), Mar^{0} (red), Jun^{0} (yellow), Nov^{0} (green), Mar^{+1} (light blue), and Jun^{+1} (dark blue), with lead times ranging from 25 (Nov^{-1}) to 6 (Jun^{+1}) months relative to Dec^{+1}. Dec^{0} denotes the first peak of El Niño/La Niña events. The solid colored curves indicate that the composite forecasts are significantly different from zero at the 95% confidence level. (right) Histograms of the Niño-3.4 index (°C) in Dec^{+1} constructed from all ensemble forecast members of all events that make up each composite, expressed as a percentage of the total number.

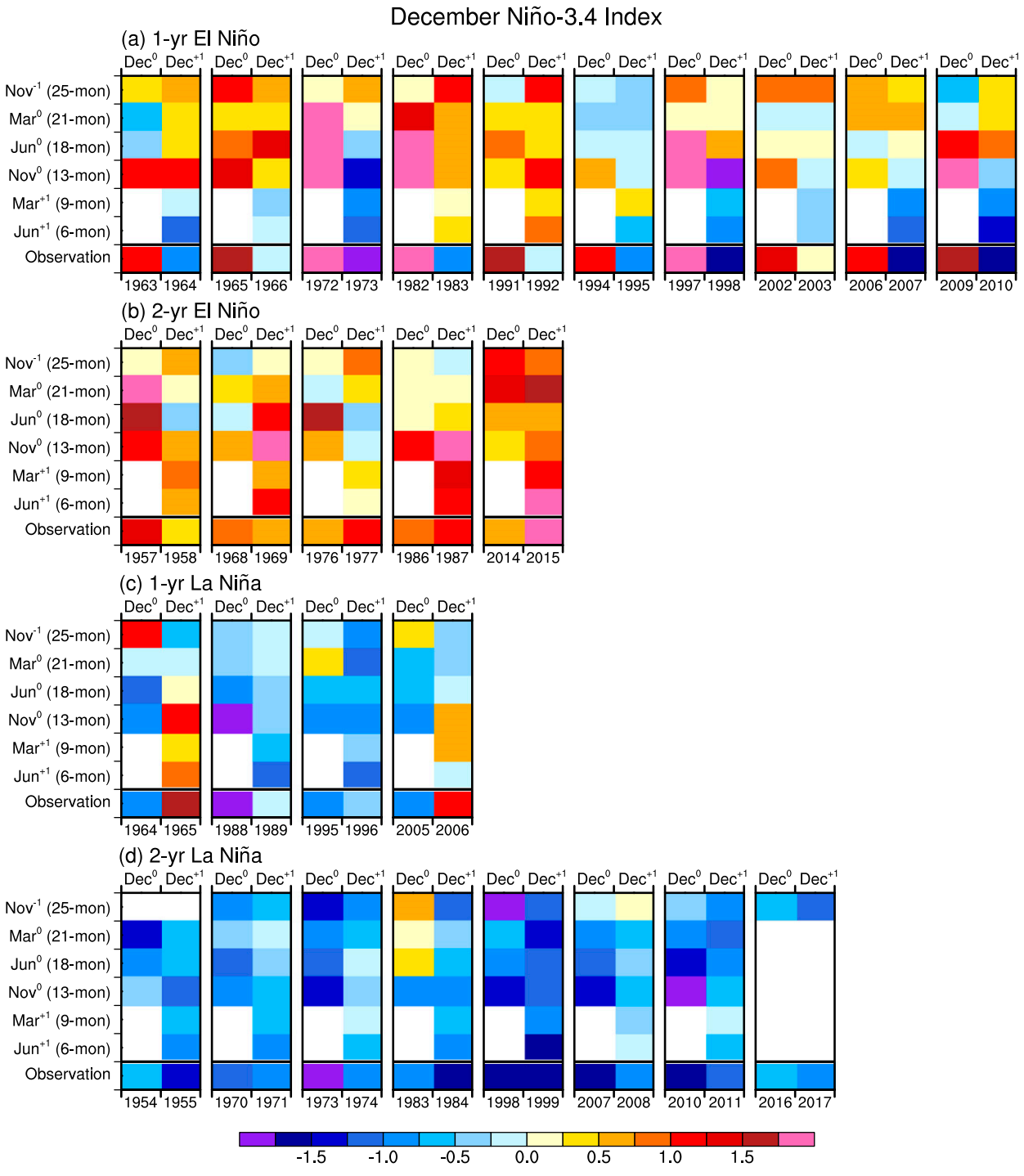

FIG. 3. Niño-3.4 index (color bar; °C) in Dec^0 (left columns) and Dec^{+1} (right columns) for individual (a) 1-yr El Niño, (b) 2-yr El Niño, (c) 1-yr La Niña, and (d) 2-yr La Niña events in observations (bottom rows) and ensemble mean forecasts (other rows) with different lead times relative to Dec^{+1} as indicated. Dec^0 denotes the first peak of El Niño/La Niña events. White boxes indicate missing data.

negative oceanic feedback, which is reflected in the Nov^0 initial thermocline states, are key to the predictions of El Niño duration, confirming that the mechanisms identified in previous diagnostic and perfect model studies also operate in the real-world forecasts (Wu et al. 2019, 2021).

The timing of delayed negative oceanic feedback also appears to be important for the predictions of La Niña duration (Fig. 5). In observations, 1-yr La Niña tends to develop around Mar^0 in the central-eastern equatorial Pacific (140°–80°W), about 3 months earlier than 2-yr La Niña. The different onset

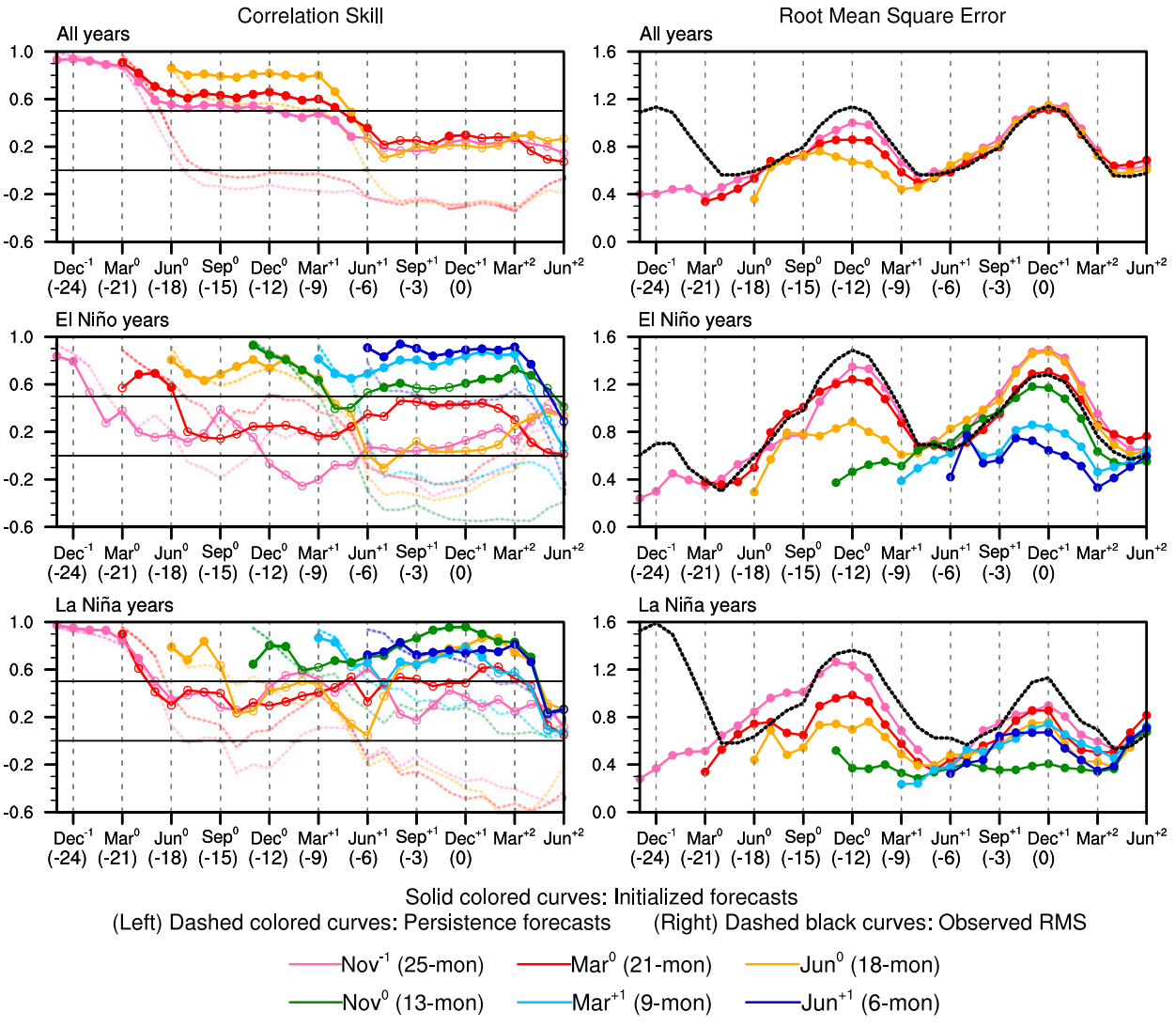

FIG. 4. (left) Correlation skill and (right) RMSE (°C) of the Niño-3.4 index in ensemble-mean forecasts initialized in different months compared to observations (solid colored curves) as a function of lead time (x axis) for (top) all years, (middle) El Niño years, and (bottom) La Niña years during 1954–2015. In the left panels, correlation skill values are indicated by filled circles are statistically significant at the 95% confidence level. The correlation skill of ensemble-mean forecasts is also compared with correlation skill of persistence forecasts (dashed colored curves). In the right panels, the RMSE of ensemble-mean forecasts is compared with RMS of the observed Niño-3.4 index (dashed black curves). The forecasts are initialized in Nov^{-1} (pink), Mar^{0} (red), Jun^{0} (yellow), Nov^{0} (green), Mar^{+1} (light blue), and Jun^{+1} (dark blue), with lead times ranging from 25 (Nov^{-1}) to 6 (Jun^{+1}) months relative to Dec^{+1}. Dec^{0} denotes the first peak of El Niño/La Niña events.

timing results in opposite signs of thermocline depth anomalies in the western equatorial Pacific in Nov^{0}. When initialized with these distinct oceanic conditions in Nov^{0}, the CESM1 successfully predicts the evolution of 1- and 2-yr La Niña in year +1. The Nov^{0} oceanic states are also strongly influenced by the magnitude of thermocline shoaling across the equatorial Pacific in the preceding boreal spring–summer, which is in turn related to the amplitude of preceding El Niño. In the 2-yr La Niña forecasts, the greater initial shoaling of the thermocline prevents the delayed oceanic feedback from reversing the sign of thermocline depth anomalies in the eastern equatorial Pacific.

The Nov^{0}-initialized forecasts predict the early termination of both 1-yr El Niño and La Niña events, but the timing is a few months later than in observations (Fig. 5). For example, the SST warming in the western-central Pacific associated with 1-yr El Niño is replaced by SST cooling in late boreal spring in observation but persists into boreal summer in the forecasts. Compared to observations, the predicted equatorial SST and wind anomalies extend too far west and linger too long into summer of year +1 over the western Pacific. The westward displacement of equatorial anomalies may make surface winds over the western equatorial Pacific less susceptible to the negative feedback from the tropical Indian Ocean via the atmospheric bridge and delay the event termination (Okumura and Deser, 2010; Okumura et al. 2011; Ohba and Watanabe 2012). The westward displacement of equatorial anomalies is, in turn, likely caused by too strong Pacific cold tongue in CESM1, which

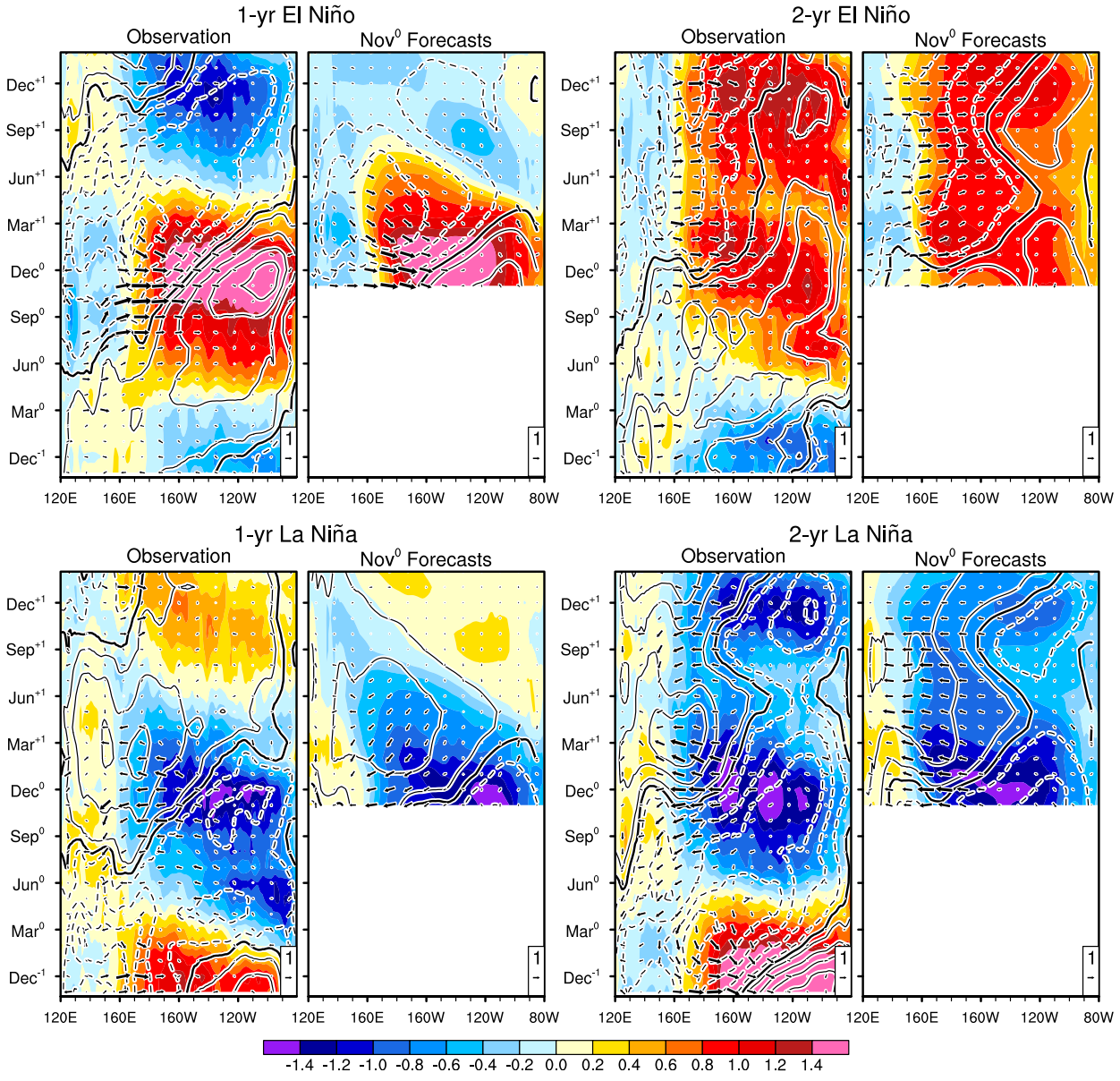

FIG. 5. Longitude–time sections of SST (°C; shading), thermocline depth (contours at intervals of 8 m starting at ±4 m; zero contours thickened and negative contours dashed), and surface wind (m s^{-1}; vectors) anomalies in the equatorial Pacific (3°S–3°N) composited for 1- and 2-yr El Niño and La Niña events in observations and ensemble-mean forecasts initialized in Nov^0. The thermocline depth anomalies are smoothed with a 1–2–1 filter in the time direction and a 9-point running-mean filter in the longitudinal direction in both observations and forecasts. Dec^0 denotes the first peak of El Niño/La Niña events. The statistical significance of these anomalies is shown in Fig. S5.

acts to shift atmospheric convection anomalies to the west (Ham and Kug 2012; Bayr et al. 2018). In support of this notion, the Jun^0-initialized forecasts show an even more pronounced bias for protracted 1-yr El Niño and La Niña (cf. Fig. 8 and Fig. S4), because the cold tongue bias develops faster in forecasts initialized during the equatorial cold season compared to those initialized in other seasons (Fig. S5; Siongco et al. 2020).

Besides the oceanic feedback, observed surface wind anomalies over the western equatorial Pacific show distinct evolutions after the first peak of 1- and 2-yr El Niño and La Niña events (Fig. 5). In particular, observed surface wind anomalies over the western equatorial Pacific decay quickly after the peak of 1-yr events but persist through year +1 of 2-yr events. The Nov^0-initialized forecasts simulate the different evolution of surface wind anomalies for 1- and 2-yr events, although the 1-yr events show a slower decay compared to observations, consistent with the slower termination of these events in the model.

To examine the causes of different wind evolutions, we compare the spatial patterns of SST and surface wind anomalies between 1- and 2-yr events during Nov^0–Dec^0 (Fig. 6; see Fig. S6 for the statistical significance of these composites). In observations, the equatorial Pacific warming is weaker in 2-yr

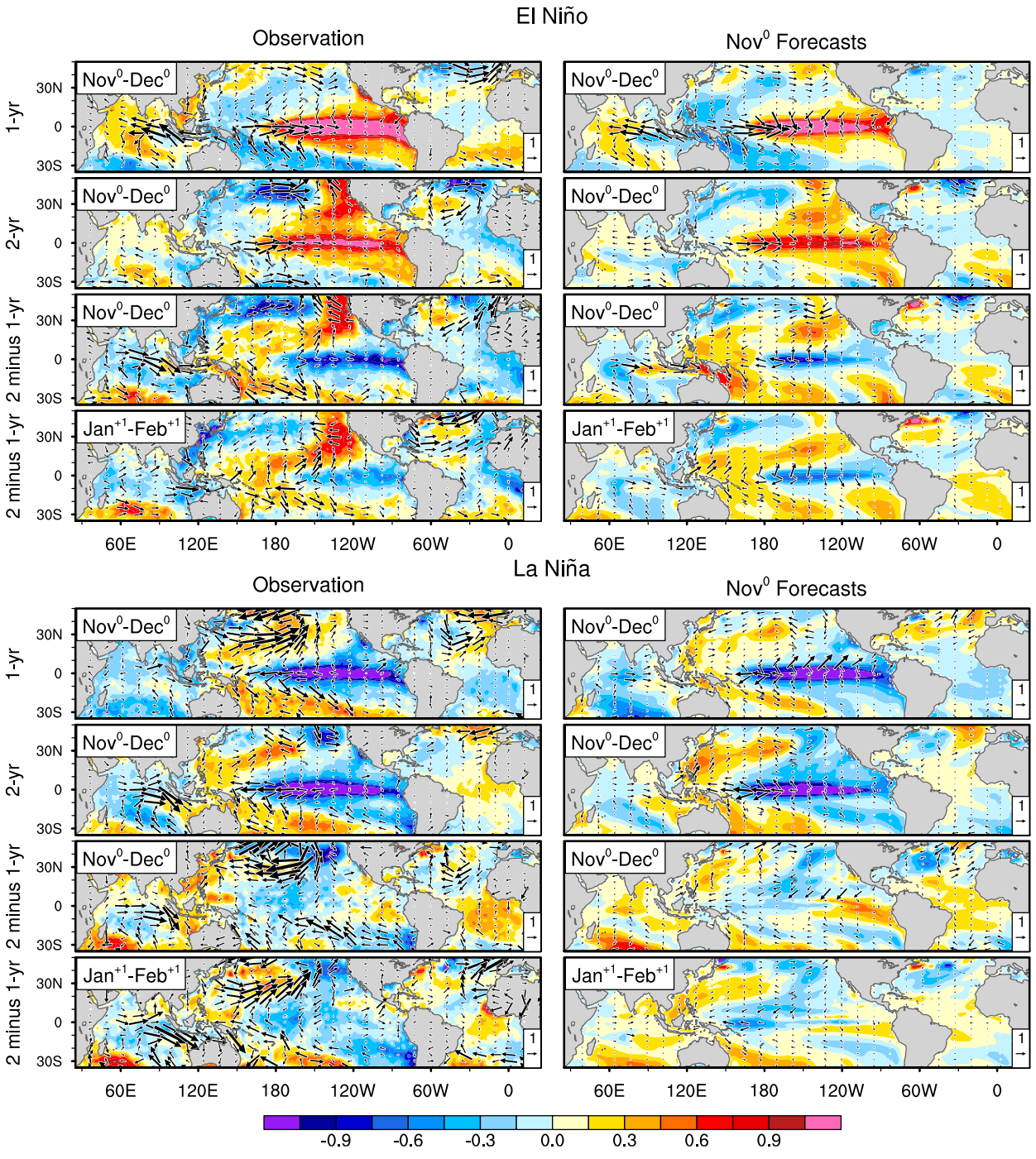

FIG. 6. Maps of SST (°C; shading) and surface wind anomalies (m s^{-1}; vectors) composited for (top) El Niño and (bottom) La Niña based on (left) observations and (right) ensemble-mean forecasts initialized in Nov^0. For El Niño and La Niña maps, the top rows show results for 1-yr events, second rows for 2-yr events, and third rows for their difference (2-yr minus 1-yr), all during Nov^0–Dec^0. The bottom rows show the difference between 2- and 1-yr events during Jan^{+1}-Feb^{+1}. The statistical significance of these anomalies is shown in Fig. S6.

than 1-yr El Niño, with the center of warming shifted slightly to the west. The tropical Atlantic and Indian Oceans also warm less in 2-yr El Niño, presumably due to the late onset and weaker amplitude of equatorial Pacific warming. Another striking difference is the SST warming in the northeast tropical Pacific and off the west coast of the United States and Mexico in 2-yr El Niño, which is nearly absent in 1-yr El Niño. The difference maps between 2- and 1-yr El Niño events display the northeast tropical Pacific warming and associated southwesterly wind anomalies in Nov^0–Dec^0. These extratropical

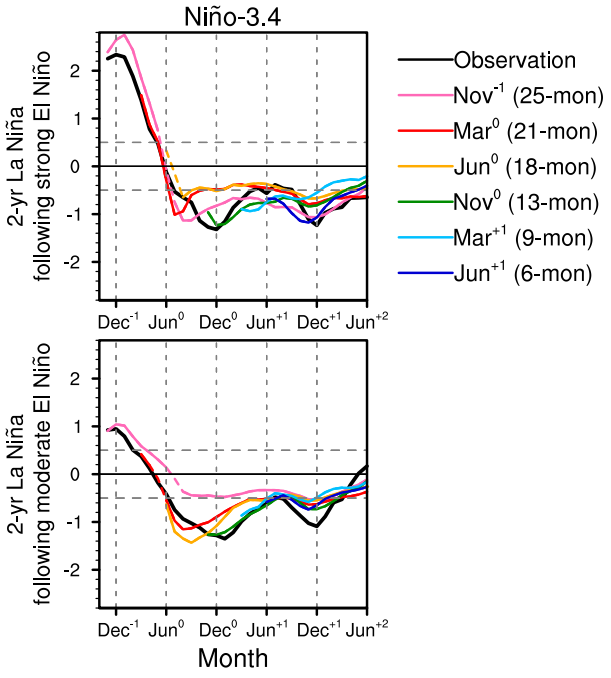

FIG. 7. Time series of the Niño-3.4 index (°C) in observations (black curves) and ensemble-mean forecasts (colored curves) composited for 2-yr La Niña events following (top) strong (1972, 1982, 1997, and 2015) and (bottom) moderate (1953, 1969, 2006, and 2009) El Niño events. The preceding El Niño is considered to be strong (moderate) when the Dec^{-1} Niño-3.4 index is >2.0°C (0.5°–2.0°C). The forecasts are initialized in Nov^{-1} (pink), Mar^{0} (red), Jun^{0} (yellow), Nov^{0} (green), Mar^{+1} (light blue), and Jun^{+1} (dark blue), with lead times ranging from 25 (Nov^{-1}) to 6 months (Jun^{+1}) relative to Dec^{+1}. Dec^{0} denotes the first peak of El Niño/La Niña events. The solid colored curves indicate that the composite forecasts are significantly different from zero at the 95% confidence level.

anomalies extend to the western equatorial Pacific in Jan^{+1}–Feb^{+1}, indicative of the role of the North Pacific meridional mode (NPMM; e.g., Vimont et al. 2001; Anderson 2003; Chang et al. 2007; Alexander et al. 2010). The SST states in Nov^{0}–Dec^{0} and subsequent equatorward propagation associated with the NPMM are well captured by the Nov^{0}-initialized forecasts, although the northeast tropical Pacific warming is weaker compared to observations. Similar differences are found between 2- and 1-yr La Niña events in both observations and the Nov^{0}-initialized forecasts, except that the amplitude of equatorial Pacific cooling is comparable between 2- and 1-yr events and the equatorward propagation of northeast tropical Pacific cooling is less clear in observations. These results suggest that in addition to the tropical interbasin adjustments the NPMM plays an important role in maintaining surface wind anomalies over the western equatorial Pacific during 2-yr El Niño and La Niña. The processes that cause the different initial NPMM states between 1- and 2-yr events in the first place remain unclear, which could be related to the internal atmospheric variability over the North Pacific or the tropical SST forcing (Capotondi et al. 2019; Stuecker 2018; Wu et al. 2019; Fang and Yu 2020). The North Pacific wind anomalies in the 2-yr El Niño and 1-yr La Niña forecasts show different patterns from observations. We note that the observational composites could be strongly influenced by internal atmospheric variability due to the small sample size (Fig. S6; Deser et al. 2017).

c. *Multiyear predictability of 2-yr La Niña*

The CESM1 shows high skill in predicting 2-yr La Niña events with lead times up to 25 months (Fig. 2). DiNezio et al. (2017a,b) suggest that the multiyear predictability of 2-yr La Niña arises from large initial shoaling of the equatorial Pacific thermocline caused by the preceding strong El Niño, but not all observed 2-yr La Niña events are preceded by strong El Niño. To explore other factors affecting the predictability, we further classify 2-yr La Niña events into those preceded by strong and moderate El Niño (Fig. 7). Here, the preceding El Niño is considered to be strong (moderate) when the smoothed Dec^{-1} Niño-3.4 index exceeds 2.0°C (0.5°–2.0°C). In agreement with DiNezio et al. (2017a,b), the CESM1 predicts 2-yr La Niña when initialized around the peak of strong El Niño in Nov^{-1}. The Nov^{-1}-initialized forecasts fail to predict the onset of 2-yr La Niña preceded by moderate El Niño, but the forecasts initialized after Mar^{0} consistently predict the development and duration of these events. This result is in contrast to the 1-yr La Niña forecasts initialized in and after Mar^{0}, which consistently predict the event termination in year +1 while the amplitude of the preceding El Niño is comparable (i.e., moderate; Fig. 2). Thus, there seem to be important factors other than the amplitude of preceding El Niño that affect the development and duration of La Niña events.

Figure 8 shows the temporal evolution of ocean–atmosphere anomalies in the equatorial Pacific, the tropical North Atlantic, and the tropical Indian Ocean for composites of 2-yr La Niña preceded by strong El Niño, 2-yr La Niña preceded by moderate El Niño and all 1-yr La Niña events, based on observations and the ensemble forecasts initialized between Nov^{-1} and Nov^{0} (see Fig. S7 for the statistical significance of these composites). When initialized with strong El Niño conditions in Nov^{-1}, the CESM1 predicts the evolution of the tropical ocean–atmosphere system in the subsequent two years of La Niña surprisingly well, comparable to the forecasts initialized in later months. In both observations and the Nov^{-1}-initialized forecasts, strong El Niño causes not only large shoaling of the equatorial Pacific thermocline, but also strong warming of the tropical Atlantic and Indian Oceans, which delay the interbasin atmospheric adjustments to La Niña cooling and maintain the easterly wind anomalies. As stated earlier, the CESM1 first predicts the development and duration of 2-yr La Niña preceded by moderate El Niño when initialized in Mar^{0}. The development and duration of 1-yr La Niña are not predicted until Jun^{0}, when the thermocline begins to shoal in the central-eastern equatorial Pacific. Compared to 1-yr La Niña, both observed and predicted 2-yr La Niña preceded by moderate El Niño shows stronger equatorial Pacific cooling, with the center displaced to the west. Thus, the amplitude and location of equatorial Pacific cooling appear to affect the La Niña duration and its predictability. It is interesting to note that the tropical North Atlantic is warmer during Nov^{0}–Apr^{0}

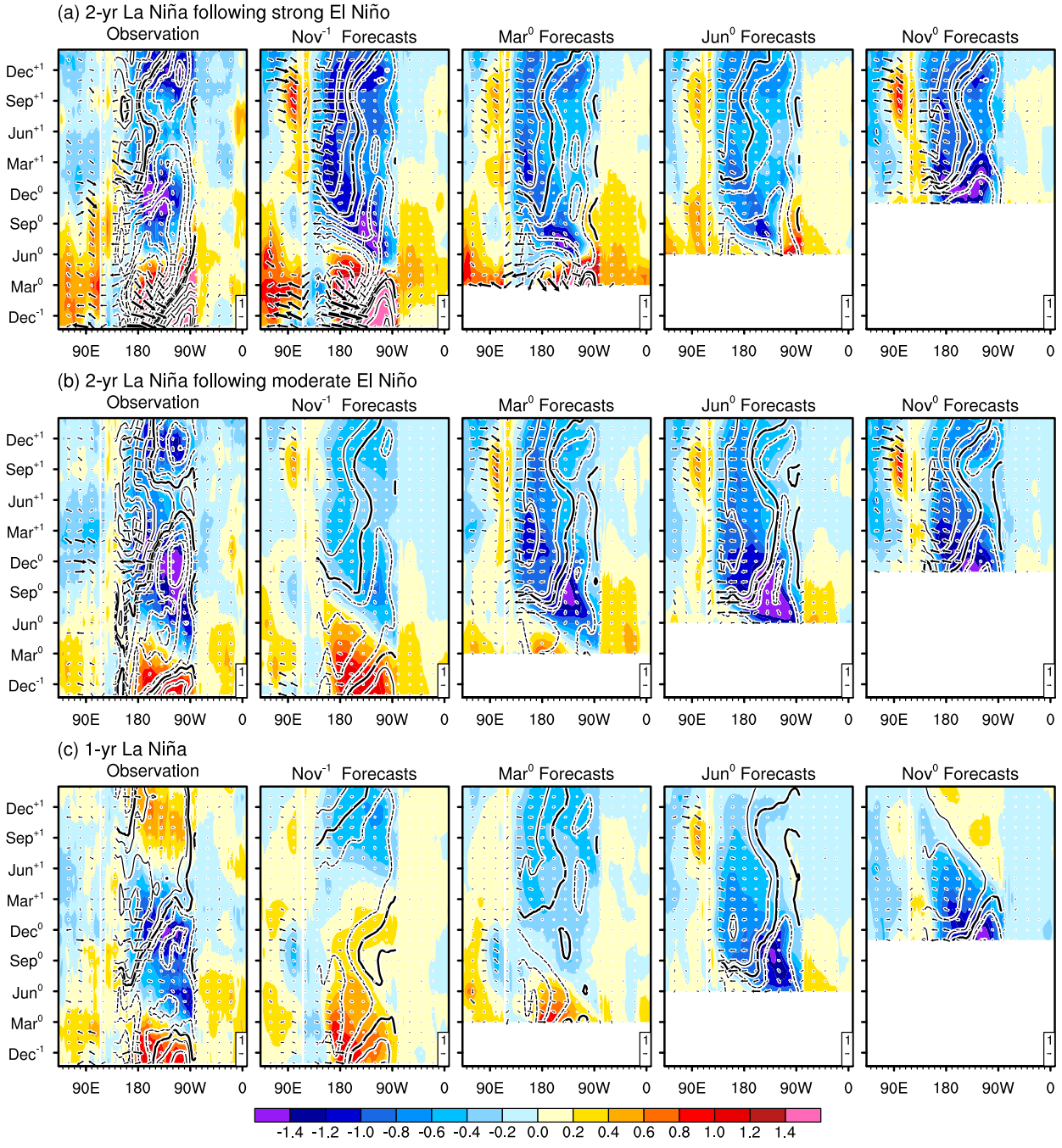

FIG. 8. Longitude–time sections of SST (°C; shading), thermocline depth (contours at intervals of 8 m starting at ±4 m; zero contours thickened and negative contours dashed), and surface wind (m s^{-1}; vectors) anomalies composited for (a) 2-yr La Niña events following strong El Niño, (b) 2-yr La Niña events following moderate El Niño events, and (c) all 1-yr La Niña events in (first column) observations and (second to fifth columns) ensemble-mean forecasts initialized in Nov^{-1}, Mar^{0}, Jun^{0}, and Nov^{0}, respectively. Dec^{0} denotes the first peak of El Niño/La Niña events. The anomalies are averaged between 3°S and 3°N in the Pacific (120°E–80°W), between 10°S and 0° in the Indian Ocean (40°–120°E), and between 0° and 20°N in the Atlantic (80°W–10°E). The thermocline depth anomalies are smoothed with a 1–2–1 filter in the time direction and a 9-point running-mean filter in the longitudinal direction in both observations and forecasts. The statistical significance of these anomalies is shown in Fig. S7.

of 2-yr La Niña preceded by moderate El Niño than 1-yr La Niña. Recent studies suggest that tropical North Atlantic SST anomalies significantly affect the development of ENSO events during boreal spring via the atmospheric bridge (Ham et al. 2013; Ham and Kug 2015). It is plausible that the magnitude of tropical North Atlantic warming in boreal spring modulates the amplitude and duration of subsequent La Niña.

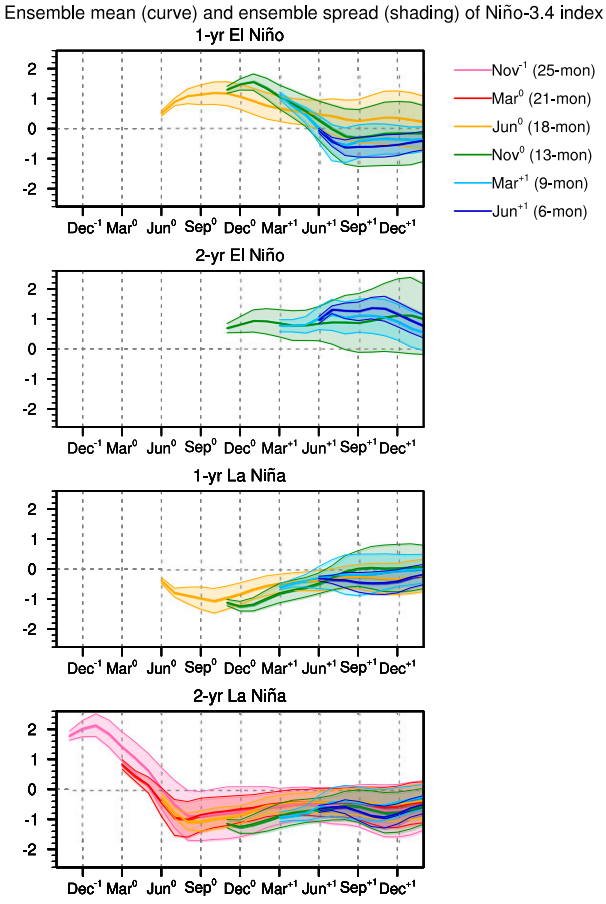

FIG. 9. Ensemble mean (curves) and spread (shading; ±1 standard deviation) of the Niño-3.4 index (°C) in forecasts initialized in Nov^{-1} (pink), Mar^{0} (red), Jun^{0} (yellow), Nov^{0} (green), Mar^{+1} (light blue), and Jun^{+1} (dark blue) composited for (first row) 1-yr El Niño, (second row) 2-yr El Niño, (third row) 1-yr La Niña, and (fourth row) 2-yr La Niña events during 1954–2015. Dec^{0} denotes the first peak of El Niño/La Niña events. The composite ensemble spread is calculated by pooling all members of the forecast ensembles for each type of events after removing the mean of each forecast ensemble from the individual members of that ensemble. Only the composite forecasts that successfully predict the duration of ENSO events are shown.

d. Sources of ensemble spread

While the ensemble-mean forecasts reveal the predictable component of the ENSO event duration, the ensemble spread provides information on the uncertainty of predictions. Figure 9 shows the growth of ensemble spread of the Niño-3.4 index around the ensemble mean as a function of lead time for forecast ensembles composited for 1- and 2-yr El Niño and La Niña events. As expected, the ensemble spread in Dec^{+1} generally becomes smaller in forecasts with shorter lead times for all four types of events, indicating decreased forecast uncertainty. The Nov^{0}-initialized forecasts, however, show larger ensemble spread in Dec^{+1} than the Jun^{0}-initialized forecasts for 1-yr El Niño and La Niña, which may be partly attributed to the larger ensemble size of the Nov^{0}-initialized forecasts (Fig. S2). It is interesting to note that the ensemble spread in Dec^{+1} is much larger for El Niño than La Niña in the forecasts initialized in or before Nov^{0}. This result suggests that the growth of ensemble spread may depend on the ensemble mean state. Similar results are found in the perfect model predictions conducted with the CESM1 and its predecessor (Wu et al. 2021; Larson and Kirtman 2019).

To identify the sources of ensemble spread of event duration, we correlate the Dec^{+1} Niño-3.4 index with global SST and SLP anomalies in the preceding months using the forecast ensembles of all El Niño and La Niña events (Fig. 10; see Fig. S8 for the statistical significance of these correlations). Before conducting the correlation analysis, we remove the ensemble mean from individual members of each forecast ensemble and then pool all forecast ensembles for each initialization month. In this way, we remove the predictable signal (given by the ensemble mean) and isolate the unpredictable component (the residual from the ensemble mean) for our analysis. Here, the state dependence of the ensemble spread is not considered but needs to be investigated in future studies. In the forecast ensembles initialized between Nov^{-1} and Nov^{0}, the ensemble spread of the Dec^{+1} Niño-3.4 index originates mainly from a meridional dipole pattern of SLP anomalies over the North Pacific in Dec^{0}–Jan^{+1} (Fig. 10b) and associated subtropical North Pacific SST anomalies that peak in Mar^{+1}–Apr^{+1} (Fig. 10c). This result indicates that wintertime atmospheric variability over the North Pacific and attendant ocean–atmosphere interactions contribute to the uncertainty of ENSO event duration, consistent with a previous study suggesting the dominant role of the NPMM in the ensemble spread of ENSO forecasts (Ma et al. 2017). In the forecasts initialized in Nov^{-1} and Mar^{0}, variability similar to the Indian Ocean dipole (IOD) mode in Sep^{0}–Oct^{0} also weakly contributes to the ensemble spread of the Dec^{+1} Niño-3.4 index (Fig. 10a). In the forecasts initialized after the first peak of El Niño and La Niña in Mar^{+1} and Jun^{+1}, the ensemble spread appears to originate mainly from atmospheric variability over the South Pacific, suggesting the role of the South Pacific meridional mode (SPMM; Fig. 10d; DiNezio et al. 2017a; Larson et al. 2018).

4. Summary and discussion

We have explored the predictability of ENSO event duration using three sets of CESM1 multiyear forecast ensembles initialized with observed oceanic and sea ice conditions on 1 March, 1 June, and 1 November of each year during 1954–2015. The CESM1 shows high predictive skill of ENSO event duration with lead times ranging from 6 to 25 months. In particular, the forecasts initialized in Nov^{0} near the first peak of El Niño and La Niña can skillfully predict whether the events terminate or persist through the following year with a lead time of 13 months. The predictability arises from the timing and magnitude of delayed negative oceanic feedbacks and interbasin adjustments, which are reflected in the initial thermocline depth and SST anomalies. In addition, subtropical North Pacific SST anomalies associated with the NPMM contribute to the predictability of ENSO event duration by affecting surface winds over the western equatorial Pacific. The occurrence of multiyear La Niña events can be predicted with lead times up to 25 months. Multiyear La Niña events preceded by strong El Niño are predicted with the longest lead time of 25 months, owing to large

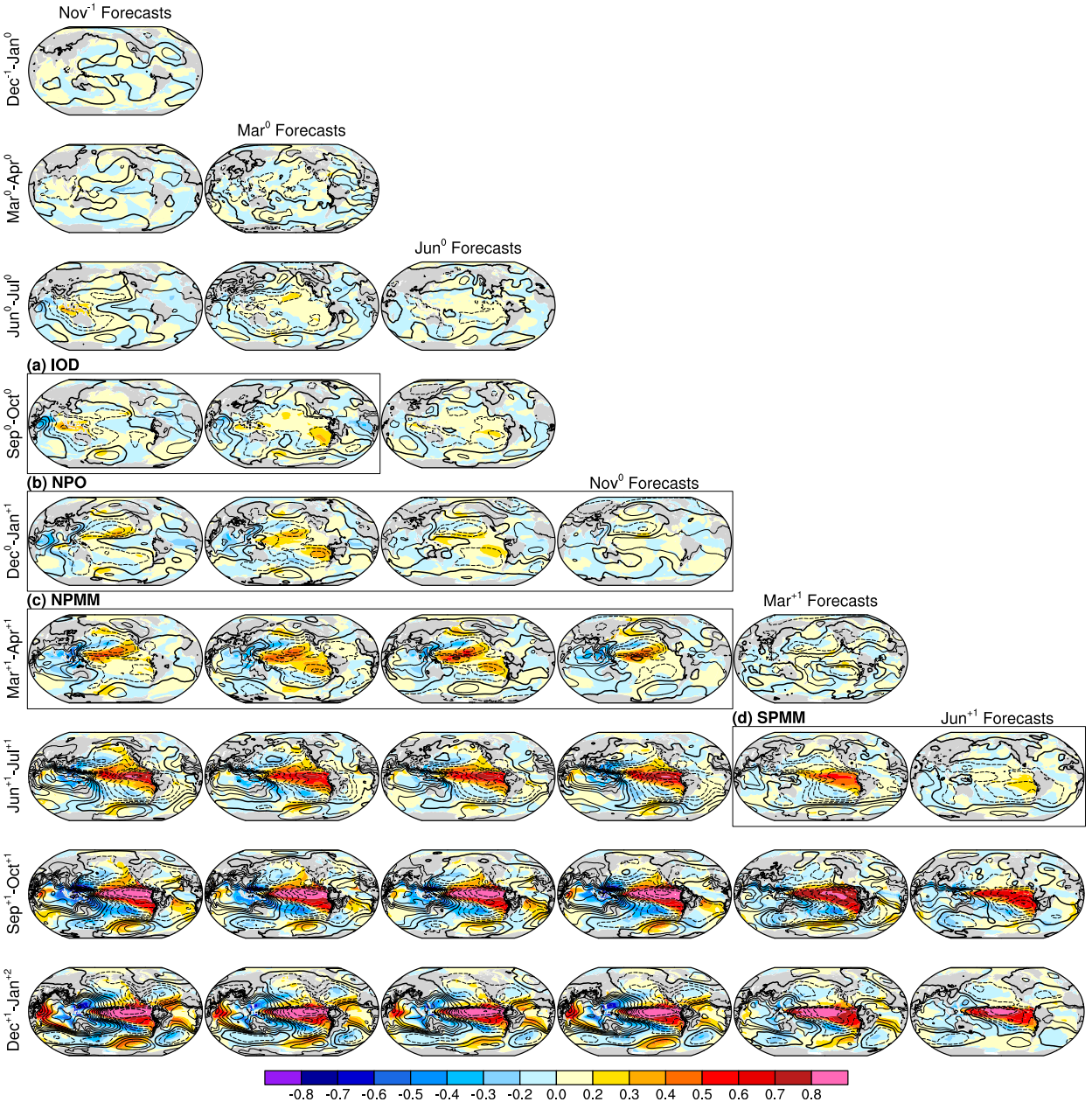

FIG. 10. Correlation maps of SST (color shading) and sea level pressure (contours at intervals of 0.1; zero contours thickened and negative contours dashed) anomalies with the Niño-3.4 index in Dec^{+1} from the ensemble forecasts as a function of lead time [columns: from (left) Nov^{-1} to (right) Jun^{+1} initialized forecasts] and verification time [rows: from (top) Dec^{-1}–Jan^{0} to (bottom) Dec^{+1}–Jan^{+2}]. All members of the forecast ensembles for all El Niño and La Niña years are pooled together after removing the mean of each forecast ensemble from the individual members of that ensemble. The boxes with labels (a)–(d) are used to denote the different processes that contribute to the ensemble spread described in the text. The statistical significance of these anomalies is shown in Fig. S8.

adjustments of the equatorial Pacific thermocline and interbasin SSTs associated with the preceding El Niño, in agreement with DiNezio et al. (2017b). When La Niña events are preceded by moderate-to-weak El Niño, springtime SST warming in the tropical North Atlantic may provide long-term predictability of La Niña duration, although the role of oceanic conditions in different ocean basins requires further investigation.

The magnitude of error growth in our 2-yr forecasts shows dependency on both lead times and ensemble mean state. The forecast uncertainty is reduced in forecasts with shorter lead times and is smaller for La Niña events than El Niño events. We investigated the general source of forecast error growth without considering these dependencies. The forecast error growth of event duration originates mainly from wintertime

atmospheric variability over the North Pacific around the first peak of El Niño and La Niña (Dec^0–Jan^{+1}) and attendant air–sea interactions in the tropical Pacific. In the forecasts initialized in Jun^0, unforced variability of the IOD in the first boreal fall also contributes to the ensemble spread. In the forecasts initialized after the first peak of El Niño and La Niña (Mar^{+1} and Jun^{+1}), the error growth of event duration is associated with atmospheric variability over the South Pacific during boreal spring to summer. The forecast errors originating from these tropical and extratropical phenomena grow faster during late boreal spring to summer than other seasons, when the seasonal cold tongue develops in the equatorial Pacific. The forecast errors are also likely caused by intraseasonal wind variability over the western equatorial Pacific (e.g., Menkes et al. 2014; Puy et al. 2017), which needs to be investigated in future research.

The predictability of ENSO event duration primarily arises from surface and subsurface oceanic conditions in the equatorial Pacific, which are also key to the predictability of onset and amplitude of ENSO events (e.g., Wyrtki 1975; Meinen and McPhaden 2000; Chen et al. 2004; Planton et al. 2018; Larson and Kirtman 2019). However, in our CESM1 forecasts, the duration of ENSO events can be predicted with longer lead times than their first onset and peak phases. This result indicates that when the equatorial Pacific system is in an El Niño or La Niña state, the ocean–atmosphere dynamics internal to the system, particularly the timing and magnitude of subsurface oceanic processes in the equatorial Pacific, is able to overcome the spring predictability barrier and provides long-term predictability. Most prominently, the strong thermocline shoaling in the equatorial Pacific induced by strong El Niño can provide 2-yr lead predictability for the subsequent multiyear La Niña, consistent with DiNezio et al. (2017b). Additional sources of predictability of ENSO event duration may come from remote ocean basins, including the tropical Indian and Atlantic as well as the extratropical Pacific, consistent with recent studies of basin interactions as summarized by Cai et al. (2019) and Amaya (2019).

The capability of the CESM1 to predict the duration of observed ENSO events is inherently lower than that in the perfect model experiments, due to model biases in simulating both the tropical Pacific mean state and ENSO (DiNezio et al. 2017a; Wu et al. 2021). As discussed earlier, the forecasts initialized with observed oceanic conditions systematically overestimate the duration of El Niño and La Niña events due to an excessively strong cold tongue and resultant westward displacement of ENSO anomalies in the equatorial Pacific in this model. The prediction skills are also degraded by errors in initial oceanic conditions. Recall that the oceanic initial conditions are derived from an ocean model simulation forced with observed atmospheric and surface flux fields, which do not perfectly agree with observations. For instance, in the forecasts of La Niña initialized with moderate El Niño conditions, the absence of observed Indian Ocean warming may contribute to the failure to predict the La Niña development in the following year (Fig. 8).

Regardless of the caveats discussed above, the results of this study indicate the potential of extending the current 12-month operational ENSO forecasts by one additional year. Our study is based on a single model and the predictability is explored only for selected initialization months. Further research is needed to explore the model and seasonal dependencies of the predictability of ENSO event duration. It is particularly important to assess the ability of models to reproduce the statistical characteristics of observed ENSO event duration using multimodel historical or control simulations, which could influence the skill of models in predicting ENSO event duration. Given the large computational costs, it may not be feasible to fully extend the operational ENSO forecasts by one additional year for all models. However, our study highlights the benefit of extending the forecasts even for selected models and selected initialization months. Multiyear ENSO forecasts will provide a new basis for predictions of prolonged climate anomalies, such as persistent drought in the southern United States and widespread flooding in Australia during multiyear La Niña events.

Acknowledgments. The authors thank the two anonymous reviewers for constructive comments and suggestions that helped to improve the manuscript. The observational datasets used in this study are obtained online: HadISST from the Met Office Hadley Center (http://www.metoffice.gov.uk/hadobs/), ECMWF Ocean Reanalysis System 4 from ftp://ftp-icdc.cen.uni-hamburg.de/EASYInit/ORA-S4, and NCEP–NCAR reanalysis from https://psl.noaa.gov/data/gridded/data.ncep.reanalysis.html. The authors thank Nan Rosenbloom for providing the oceanic and sea ice initial conditions used for the forecasts. This study is supported by the National Oceanic and Atmospheric Administration (NOAA) Climate Program Office Modeling, Analysis, Predictions, and Projections Program (NA17OAR4310149 and NA17OAR4310145) and the National Science Foundation (NSF) Physical Oceanography Program (OCE-1756883). The CESM project is supported primarily by the NSF. This material is based upon work supported by the National Center for Atmospheric Research, which is a major facility sponsored by the NSF under Cooperative Agreement 1852977.

REFERENCES

Alexander, M. A., I. Bladé, M. Newman, J. R. Lanzante, N.-C. Lau, and J. D. Scott, 2002: The atmospheric bridge: The influence of ENSO teleconnections on air–sea interaction over the global oceans. *J. Climate*, **15**, 2205–2231, https://doi.org/10.1175/1520-0442(2002)015<2205:TABTIO>2.0.CO;2.

——, D. J. Vimont, P. Chang, and J. D. Scott, 2010: The impact of extratropical atmospheric variability on ENSO: Testing the seasonal footprinting mechanism using coupled model experiments. *J. Climate*, **23**, 2885–2901, https://doi.org/10.1175/2010JCLI3205.1.

Amaya, D. J., 2019: The Pacific Meridional Mode and ENSO: A review. *Curr. Climate Change Rep.*, **5**, 296–307, https://doi.org/10.1007/s40641-019-00142-x.

An, S.-I., E. Tziperman, Y. M. Okumura, and T. Li, 2020: ENSO irregularity and asymmetry. *El Niño Southern Oscillation in a Changing Climate*, *Geophys. Monogr.*, Vol. 253, Amer. Geophys. Union, 153–172.

Anderson, B. T., 2003: Tropical Pacific sea-surface temperatures and preceding sea level pressure anomalies in the subtropical

North Pacific. *J. Geophys. Res.*, **108**, 4732, https://doi.org/10.1029/2003JD003805.

Balmaseda, M., K. Mogensen, and A. T. Weaver, 2013: Evaluation of the ECMWF ocean reanalysis system ORAS4. *Quart. J. Roy. Meteor. Soc.*, **139**, 1132–1161, https://doi.org/10.1002/qj.2063.

Barnston, A. G., M. K. Tippett, M. L. L'Heureux, S. Li, and D. G. DeWitt, 2012: Skill of real-time seasonal ENSO model predictions during 2002–11: Is our capability increasing? *Bull. Amer. Meteor. Soc.*, **93**, 631–651, https://doi.org/10.1175/BAMS-D-11-00111.1.

——, ——, M. Ranganathan, and M. L. L'Heureux, 2019: Deterministic skill of ENSO predictions from the North American multimodel ensemble. *Climate Dyn.*, **53**, 7215–7234, https://doi.org/10.1007/s00382-017-3603-3.

Bayr, T., M. Latif, D. Dommenget, C. Wengel, J. Harlaß, and W. Park, 2018: Mean-state dependence of ENSO atmospheric feedbacks in climate models. *Climate Dyn.*, **50**, 3171–3194, https://doi.org/10.1007/s00382-017-3799-2.

Bellenger, H., E. Guilyardi, J. Leloup, M. Lengaigne, and J. Vialard, 2014: ENSO representation in climate models: From CMIP3 to CMIP5. *Climate Dyn.*, **42**, 1999–2018, https://doi.org/10.1007/s00382-013-1783-z.

Cai, W., and Coauthors, 2019: Pantropical climate interactions. *Science*, **363**, eaav4236, https://doi.org/10.1126/science.aav4236.

Capotondi, A., and Coauthors, 2015: Understanding ENSO diversity. *Bull. Amer. Meteor. Soc.*, **96**, 921–938, https://doi.org/10.1175/BAMS-D-13-00117.1.

——, P. D. Sardeshmukh, E. Di Lorenzo, A. C. Subramanian, and A. J. Miller, 2019: Predictability of US West Coast ocean temperatures is not solely due to ENSO. *Sci. Rep.*, **9**, 10993, https://doi.org/10.1038/s41598-019-47400-4.

——, C. Deser, A. S. Phillips, Y. M. Okumura, and S. M. Larson, 2020: ENSO and Pacific decadal variability in the Community Earth System Model version 2. *J. Adv. Model Earth Syst.*, **12**, e2019MS002022, https://doi.org/10.1029/2019MS002022.

Chang, P., and Coauthors, 2006: Climate fluctuations of tropical coupled systems—The role of ocean dynamics. *J. Climate*, **19**, 5122–5174, https://doi.org/10.1175/JCLI3903.1.

——, L. Zhang, R. Saravanan, D. J. Vimont, J. C. H. Chiang, L. Ji, H. Seidel, and M. K. Tippett, 2007: Pacific meridional mode and El Niño–Southern Oscillation. *Geophys. Res. Lett.*, **34**, L16608, https://doi.org/10.1029/2007GL030302.

Chen, D., and M. A. Cane, 2008: El Niño prediction and predictability. *J. Comput. Phys.*, **227**, 3625–3640, https://doi.org/10.1016/j.jcp.2007.05.014.

——, ——, A. Kaplan, S. E. Zebiak, and D. Huang, 2004: Predictability of El Niño over the past 148 years. *Nature*, **428**, 733–736, https://doi.org/10.1038/nature02439.

CLIVAR, 2011: Data and bias correction for decadal climate prediction, CLIVAR Publication Series, No. 150, International CLIVAR Project Office, Southampton, United Kingdom, 4 pp., https://www.wcrp-climate.org/decadal/references/DCPP_Bias_Correction.pdf.

Deepak, S. N. R., J. S. Chowdary, A. R. Dandi, G. Srinivas, A. Parekh, C. Gnanaseelan, and R. K. Yadav, 2019: Impact of multiyear La Niña events on the South and East Asian summer monsoon rainfall in observations and CMIP5 models. *Climate Dyn.*, **52**, 6989–7011, https://doi.org/10.1007/s00382-018-4561-0.

Deser, C., I. R. Simpson, K. A. McKinnon, and A. S. Phillips, 2017: The Northern Hemisphere extratropical atmospheric circulation response to ENSO: How well do we know it and how do we evaluate models accordingly? *J. Climate*, **30**, 5059–5082, https://doi.org/10.1175/JCLI-D-16-0844.1.

DiNezio, P. N., and C. Deser, 2014: Nonlinear controls on the persistence of La Niña. *J. Climate*, **27**, 7335–7355, https://doi.org/10.1175/JCLI-D-14-00033.1.

——, ——, Y. M. Okumura, and A. Karspeck, 2017a: Predictability of 2-year La Niña events in a coupled general circulation model. *Climate Dyn.*, **49**, 4237–4261, https://doi.org/10.1007/s00382-017-3575-3.

——, and Coauthors, 2017b: A 2 year forecast for a 60–80% chance of La Niña in 2017–2018. *Geophys. Res. Lett.*, **44**, 11 624–11 635, https://doi.org/10.1002/2017GL074904.

Dommenget, D., T. Bayr, and C. Frauen, 2013: Analysis of the nonlinearity in the pattern and time evolution of El Niño Southern Oscillation. *Climate Dyn.*, **40**, 2825–2847, https://doi.org/10.1007/s00382-012-1475-0.

Fang, S.-W., and J.-Y. Yu, 2020: A control of ENSO transition complexity by tropical Pacific mean SSTs through tropical–subtropical interaction. *Geophys. Res. Lett.*, **47**, e2020GL087933, https://doi.org/10.1029/2020GL087933.

Graham, F. S., A. T. Wittenberg, J. N. Brown, S. J. Marsland, and N. J. Holbrook, 2017: Understanding the double peaked El Niño in coupled GCMs. *Climate Dyn.*, **48**, 2045–2063, https://doi.org/10.1007/s00382-016-3189-1.

Ham, Y.-G., and J.-S. Kug, 2012: How well do current climate models simulate two types of El Niño? *Climate Dyn.*, **39**, 383–398, https://doi.org/10.1007/s00382-011-1157-3.

——, and ——, 2015: Role of north tropical Atlantic SST on the ENSO simulated using CMIP3 and CMIP5 models. *Climate Dyn.*, **45**, 3103–3117, https://doi.org/10.1007/s00382-015-2527-z.

——, ——, J.-Y. Park, and F.-F. Jin, 2013: Sea surface temperature in the north tropical Atlantic as a trigger for El Niño/Southern Oscillation events. *Nat. Geosci.*, **6**, 112–116, https://doi.org/10.1038/ngeo1686.

Hazeleger, W., V. Guemas, B. Wouters, S. Corti, I. Andreu-Burillo, F. J. Doblas-Reyes, K. Wyser, and M. Caian, 2013: Multiyear climate predictions using two initialization strategies. *Geophys. Res. Lett.*, **40**, 1794–1798, https://doi.org/10.1002/grl.50355.

Hendon, H. H., E. Lim, G. Wang, O. Alves, and D. Hudson, 2009: Prospects for predicting two flavors of El Niño. *Geophys. Res. Lett.*, **36**, L19713, https://doi.org/10.1029/2009GL040100.

Hoerling, M. P., and A. Kumar, 2003: The perfect ocean for drought. *Science*, **299**, 691–694, https://doi.org/10.1126/science.1079053.

Horii, T., and K. Hanawa, 2004: A relationship between timing of El Niño onset and subsequent evolution. *Geophys. Res. Lett.*, **31**, L06304, https://doi.org/10.1029/2003GL019239.

Hunke, E. C., and W. H. Lipscomb, 2008: CICE: The Los Alamos sea ice model, documentation and software, version 4.0. Los Alamos National Laboratory Tech. Rep. LA-CC-06-012, 76 pp.

Hurrell, J., and Coauthors, 2013: The Community Earth System Model: A framework for collaborative research. *Bull. Amer. Meteor. Soc.*, **94**, 1339–1360, https://doi.org/10.1175/BAMS-D-12-00121.1.

Imada, Y., H. Tatebe, M. Ishii, Y. Chikamoto, M. Mori, M. Arai, M. Watanabe, and M. Kimoto, 2015: Predictability of two types of El Niño assessed using an extended seasonal prediction system by MIROC. *Mon. Wea. Rev.*, **143**, 4597–4617, https://doi.org/10.1175/MWR-D-15-0007.1.

Jin, E. K., and Coauthors, 2008: Current status of ENSO prediction skill in coupled ocean–atmosphere models. *Climate Dyn.*, **31**, 647–664, https://doi.org/10.1007/s00382-008-0397-3.

Kalnay, E. M., and Coauthors, 1996: The NCEP/NCAR 40-Year Reanalysis Project. *Bull. Amer. Meteor. Soc.*, **77**, 437–471,

https://doi.org/10.1175/1520-0477(1996)077<0437:TNYRP>2.0.CO;2.

Kay, J. E., and Coauthors, 2015: The Community Earth System Model (CESM) Large Ensemble Project: A community resource for studying climate change in the presence of internal climate variability. *Bull. Amer. Meteor. Soc.*, **96**, 1333–1349, https://doi.org/10.1175/BAMS-D-13-00255.1.

Kessler, W. S., 2002: Is ENSO a cycle or a series of events? *Geophys. Res. Lett.*, **29**, 2125, https://doi.org/10.1029/2002GL015924.

Kirtman, B. P., J. Shukla, M. Balmaseda, N. Graham, C. Penland, Y. Xue, and S. Zebiak, 2002: Current status of ENSO forecast skill: A report to the CLIVAR Working Group on Seasonal to Interannual Prediction. International CLIVAR Project Office Rep. 56, 24 pp.

Kumar, A., and M. P. Hoerling, 2000: Analysis of a conceptual model of seasonal climate variability and implications for seasonal prediction. *Bull. Amer. Meteor. Soc.*, **81**, 255–264, https://doi.org/10.1175/1520-0477(2000)081<0255:AOACMO>2.3.CO;2.

——, B. Jha, and H. Wang, 2014: Attribution of SST variability in global oceans and the role of ENSO. *Climate Dyn.*, **43**, 209–220, https://doi.org/10.1007/s00382-013-1865-y.

Larkin, N. K., and D. E. Harrison, 2002: ENSO warm (El Niño) and cold (La Niña) event life cycles: Ocean surface anomaly patterns, their symmetries, asymmetries, and implications. *J. Climate*, **15**, 1118–1140, https://doi.org/10.1175/1520-0442(2002)015<1118:EWENOA>2.0.CO;2.

Larson, S. M., and B. P. Kirtman, 2019: Linking preconditioning to extreme ENSO events and reduced ensemble spread. *Climate Dyn.*, **52**, 7417–7433, https://doi.org/10.1007/s00382-017-3791-x.

——, K. V. Pegion, and B. P. Kirtman, 2018: The South Pacific meridional mode as a thermally driven source of ENSO amplitude modulation and uncertainty. *J. Climate*, **31**, 5127–5145, https://doi.org/10.1175/JCLI-D-17-0722.1.

Latif, M., D. Anderson, T. Barnett, M. Cane, R. Kleeman, A. Leetmaa, J. O'Brien, A. Rosati, and E. Schneider, 1998: A review of the predictability and prediction of ENSO. *J. Geophys. Res.*, **103**, 14 375–14 393, https://doi.org/10.1029/97JC03413.

Lawrence, D. M., and Coauthors, 2011: Parameterization improvements and functional and structural advances in version 4 of the Community Land Model. *J. Adv. Model. Earth Syst.*, **3**, M03001, https://doi.org/10.1029/2011MS00045.

Lee, S.-K., P. N. DiNezio, E.-S. Chung, S.-W. Yeh, A. T. Wittenberg, and C. Wang, 2014: Spring persistence, transition and resurgence of El Niño. *Geophys. Res. Lett.*, **41**, 8578–8585, https://doi.org/10.1002/2014GL062484.

L'Heureux, M. L., M. K. Tippett, and A. G. Barnston, 2015: Characterizing ENSO coupled variability and its impact on North American seasonal precipitation and temperature. *J. Climate*, **28**, 4231–4245, https://doi.org/10.1175/JCLI-D-14-00508.1.

——, A. F. Z. Levine, M. Newman, C. Ganter, J.-J. Luo, M. K. Tippett, and T. N. Stockdale, 2020: ENSO prediction. *El Niño Southern Oscillation in a Changing Climate*, *Geophys. Monogr.*, Vol. 253, Amer. Geophys. Union, 227–246.

Luo, J.-J., G. Liu, H. Hendon, O. Alves, and T. Yamagata, 2017: Interbasin sources for two-year predictability of the multiyear La Niña event in 2010–2012. *Sci. Rep.*, **7**, 2276, https://doi.org/10.1038/s41598-017-01479-9.

Ma, J., S.-P. Xie, and H. Xu, 2017: Contributions of the North Pacific meridional mode to ensemble spread of ENSO prediction. *J. Climate*, **30**, 9167–9181, https://doi.org/10.1175/JCLI-D-17-0182.1.

McPhaden, M. J., and X. Zhang, 2009: Asymmetry in zonal phase propagation of ENSO sea surface temperature anomalies. *Geophys. Res. Lett.*, **36**, L13703, https://doi.org/10.1029/2009GL038774.

Meehl, G. A., and H. Teng, 2012: Case studies for initialized decadal hindcasts and predictions for the Pacific region. *Geophys. Res. Lett.*, **39**, L22705, https://doi.org/10.1029/2012GL053423.

Meinen, C. S., and M. J. McPhaden, 2000: Observations of warm water volume changes in the equatorial Pacific and their relationship to El Niño and La Niña. *J. Climate*, **13**, 3551–3559, https://doi.org/10.1175/1520-0442(2000)013<3551:OOWWVC>2.0.CO;2.

Menkes, C. E., M. Lengaigne, J. Vialard, M. Puy, P. Marchesiello, S. Cravatte, and G. Cambon, 2014: About the role of westerly wind events in the possible development of an El Niño in 2014. *Geophys. Res. Lett.*, **41**, 6476–6483, https://doi.org/10.1002/2014GL061186.

Neale, R. B., and Coauthors, 2012: Description of the NCAR Community Atmosphere Model (CAM 5.0). NCAR Tech. Note NCAR/TN-486+STR, 274 pp., www.cesm.ucar.edu/models/cesm1.0/cam/docs/description/cam5_desc.pdf.

Neelin, J. D., D. S. Battisti, A. C. Hirst, F.-F. Jin, Y. Wakata, T. Yamagata, and S. E. Zebiak, 1998: ENSO theory. *J. Geophys. Res.*, **103**, 14 261–14 290, https://doi.org/10.1029/97JC03424.

Ohba, M., and H. Ueda, 2009: Role of nonlinear atmospheric response to SST on the asymmetric transition process of ENSO. *J. Climate*, **22**, 177–192, https://doi.org/10.1175/2008JCLI2334.1.

——, and M. Watanabe, 2012: Role of the Indo-Pacific interbasin coupling in predicting asymmetric ENSO transition and duration. *J. Climate*, **25**, 3321–3335, https://doi.org/10.1175/JCLI-D-11-00409.1.

——, D. Nohara, and H. Ueda, 2010: Simulation of asymmetric ENSO transition in WCRP CMIP3 multimodel experiments. *J. Climate*, **23**, 6051–6067, https://doi.org/10.1175/2010JCLI3608.1.

Okumura, Y. M., and C. Deser, 2010: Asymmetry in the duration of El Niño and La Niña. *J. Climate*, **23**, 5826–5843, https://doi.org/10.1175/2010JCLI3592.1.

——, M. Ohba, C. Deser, and H. Ueda, 2011: A proposed mechanism for the asymmetric duration of El Niño and La Niña. *J. Climate*, **24**, 3822–3829, https://doi.org/10.1175/2011JCLI3999.1.

——, P. N. DiNezio, and C. Deser, 2017: Evolving impacts of multiyear La Niña events on atmospheric circulation and U.S. drought. *Geophys. Res. Lett.*, **44**, 11 614–11 623, https://doi.org/10.1002/2017GL075034.

Planton, Y., J. Vialard, E. Guilyardi, M. Lengaigne, and T. Izumo, 2018: Western Pacific oceanic heat content: A better predictor of La Niña than of El Niño. *Geophys. Res. Lett.*, **45**, 9824–9833, https://doi.org/10.1029/2018GL079341.

——, and Coauthors, 2021: ENSO evaluation in climate models: The CLIVAR 2020 metrics package. *Bull. Amer. Meteor. Soc.*, **102**, E193–E217, https://doi.org/10.1175/BAMS-D-19-0337.1.

Puy, M., and Coauthors, 2017: Influence of westerly wind events stochasticity on El Niño amplitude: The case of 2014 vs. 2015. *Climate Dyn.*, **52**, E193–E217, https://doi.org/10.1007/s00382-017-3938-9.

Rayner, N. A., D. E. Parker, E. B. Horton, C. K. Folland, L. Alexandre, D. P. Rowell, E. C. Kent, and A. Kaplan, 2003: Global analyses of sea surface temperature, sea ice, and night marine air temperature since the late nineteenth century. *J. Geophys. Res.*, **108**, 4407, https://doi.org/10.1029/2002JD002670.

Scaife, A. A., and Coauthors, 2014: Skillful long-range prediction of European and North American winters. *Geophys. Res. Lett.*, **41**, 2514–2519, https://doi.org/10.1002/2014GL059637.

Shukla, J., and Coauthors, 2000: Dynamical seasonal prediction. *Bull. Amer. Meteor. Soc.*, **81**, 2593–2606, https://doi.org/10.1175/1520-0477(2000)081<2593:DSP>2.3.CO;2.

Siongco, A. C., H.-Y. Ma, S. A. Klein, S. Xie, A. R. Karspeck, K. Raeder, and J. L. Anderson, 2020: A hindcast approach to diagnosing the equatorial Pacific cold tongue SST bias in CESM1. *J. Climate*, **33**, 1437–1453, https://doi.org/10.1175/JCLI-D-19-0513.1.

Smith, R. D., and Coauthors, 2010: The Parallel Ocean Program (POP) reference manual. Los Alamos National Laboratory Tech. Rep. LAUR-10-01853, 140 pp.

Stuecker, M. F., 2018: Revisiting the Pacific Meridional Mode. *Sci. Rep.*, **8**, 3216, https://doi.org/10.1038/s41598-018-21537-0.

Taschetto, A. S., C. C. Ummenhofer, M. F. Stuecker, D. Dommenget, K. Ashok, R. R. Rodrigues, and S.-W. Yeh, 2020: El Niño–Southern Oscillation atmospheric teleconnections. *El Niño Southern Oscillation in a Changing Climate*, *Geophys. Monogr.*, Vol. 253, Amer. Geophys. Union, 309–335.

Torrence, C., and P. J. Webster, 1998: The annual cycle of persistence in the El Niño–Southern Oscillation statistics. *Quart. J. Roy. Meteor. Soc.*, **124**, 1985–2004, https://doi.org/10.1002/QJ.49712455010.

Trenberth, K. E., G. W. Branstator, D. Karoly, A. Kumar, N.-C. Lau, and C. Ropelewski, 1998: Progress during TOGA in understanding and modeling global teleconnections associated with tropical sea surface temperatures. *J. Geophys. Res.*, **103**, 14 291–14 324, https://doi.org/10.1029/97JC01444.

Vimont, D. J., D. S. Battisti, and A. C. Hirst, 2001: Footprinting: A seasonal connection between the tropics and mid-latitudes. *Geophys. Res. Lett.*, **28**, 3923–3926, https://doi.org/10.1029/2001GL013435.

Wallace, J. M., E. M. Rasmusson, T. P. Mitchell, V. E. Kousky, E. S. Sarachik, and H. von Storch, 1998: On the structure and evolution of ENSO related climate variability in the tropical Pacific: Lessons from TOGA. *J. Geophys. Res.*, **103**, 14 241–14 259, https://doi.org/10.1029/97JC02905.

Wang, C., and J. Picaut, 2004: Understanding ENSO physics—A review. *Earth's Climate: The Ocean–Atmosphere Interaction*, *Geophys. Monogr.*, No. 147, Amer. Geophys. Union, 21–48.

Wu, B., T. Li, and T. Zhou, 2010: Asymmetry of atmospheric circulation anomalies over the western North Pacific between El Niño and La Niña. *J. Climate*, **23**, 4807–4822, https://doi.org/10.1175/2010JCLI3222.1.

Wu, X., Y. M. Okumura, and P. N. DiNezio, 2019: What controls the duration of El Niño and La Niña events? *J. Climate*, **32**, 5941–5965, https://doi.org/10.1175/JCLI-D-18-0681.1.

——, ——, and ——, 2021: Predictability of El Niño duration based on the onset timing. *J. Climate*, **34**, 1351–1366, https://doi.org/10.1175/JCLI-D-19-0963.1.

Wyrtki, K., 1975: El Niño—The dynamic response of the equatorial Pacific Ocean to atmospheric forcing. *J. Phys. Oceanogr.*, **5**, 572–584, https://doi.org/10.1175/1520-0485(1975)005<0572:ENTDRO>2.0.CO;2.

Yeager, S. G., A. Karspeck, G. Danabasoglu, J. Tribbia, and H. Teng, 2012: A decadal prediction case study: Late twentieth-century North Atlantic Ocean heat content. *J. Climate*, **25**, 5173–5189, https://doi.org/10.1175/JCLI-D-11-00595.1.

——, ——, and ——, 2015: Predicted slowdown in the rate of Atlantic sea ice loss. *Geophys. Res. Lett.*, **42**, 10 704–10 713, https://doi.org/10.1002/2015GL065364.

——, and Coauthors, 2018: Predicting near-term changes in the Earth system: A large ensemble of initialized decadal prediction simulations using the Community Earth System Model. *Bull. Amer. Meteor. Soc.*, **99**, 1867–1886, https://doi.org/10.1175/BAMS-D-17-0098.1.